University of Connecticut

HEALTH MONITORING OF STRUCTURES WITH CABLE MEMBERS UNDER TENSION

Senior Design Team

Eric Snapper - Electrical & Computer Engineering

Jeffrey Urban – Electrical & Computer Engineering

Christopher Von Kohorn – Mechanical Engineering

Sponsor

Dr. Jonathan Russell - Civil Engineering, Coast Guard Academy

Advisors

Dr. Sung Yeul Park – Electrical Engineering

Dr. Kevin Murphy – Mechanical Engineering

Dr. John Bennett – Mechanical Engineering

Dr. Rich Dino – Business / Management

May 2010 | ECE 4902

1. Table of Contents

Appendixes are in separate documents.

2. Abstract

The monitoring of cable tension in radio towers is important to ensure a tower's structural integrity. Improper tension can result in damage to the tower or possible collapse. The current methods for measuring tension of these cables are mechanical in nature. These methods are either very inaccurate, or require a team of technicians working multiple days with expensive, heavy equipment. Vibrational methods to determine tension have been successfully applied to other cable structures, such as bridge supports. These methods do not directly translate to cable stayed towers, because they cannot account for the significant sag and distributed, heavy non-conducting elements found on these cables. Our sponsor Dr. Jonathan Russell, a professor of civil engineering at the Coast Guard Academy, has defined a unique structural analysis algorithm to predict resonant frequencies for given tensions from the geometry and physical properties of the cable structure. Our team has investigated the characteristics of these structures and automated the process of vibrational measurement and analysis. We have developed both PC based and (self-contained) embedded prototypes to determine resonant frequencies for comparison to predicted frequencies as a method to determine cable tension.

3. Introduction

Variables and Constants:

A – The unstrained cross-sectional area of the cable

D – The weight density of the cable

E – The modulus of elasticity of the cable

F – The cable force measured by the force transducer

f – The static frictional force

g – The gravitational acceleration constant (32.2 ft/sec^2)

H – The Vertical component of tension of the cable

h – The Vertical span between the base of the cable and the structure to which it is attached

I – The Moment of Inertia

i – The Horizontal span between the base of the cable and the structure to which it is attached

k – The static coefficient of friction

L – The unstrained length of the cable

M – Bending Moment

Tb – The tension calculated at the base of the cable

Tt – The tension calculated at the top of the cable

V – The Horizontal component of tension in the cable

W – The weight of the lab setup base structure

y – The deflection of an aluminum beam due to bending

θ **–** The angle between the bottom test end of the test cable and the base structure

Terminology:

Accelerometer – An instrument for measuring acceleration

ADC – (Analog Digital Converter) A circuit that samples voltage signals and outputs digital values

Aliasing – Distortions in data that occur when reflections of elements above the maximum frequency are represented within the frequency range under consideration

Amplitude quantization – The discrete sampling of signal amplitude

Anti-Galloping Cable – A cable attached to possible Galloping Cable to restrain it

'As Built Print' – A structural print of the broadcasting tower with the measurements of how the tower was built as opposed to how it was planned

Bin Spacing – The difference in frequency between subsequent magnitudes in the frequency domain output from an FFT

Bit Width – The number of binary digits that can be represented by a given variable

Curve Fitting – To construct a curve with the best fit to a series of data points

Discretized – To be divided into distinct elements spaced by multiples of fixed intervals

Dithering – The alternating of a signal among LSB (least-significant-bit) values that when averaged over time, offers a higher level of accuracy than individual values

Embedded – Contained within a system

Fast Fourier Transform (FFT) – An algorithm to convert signals from the time domain to a frequency spectrum

Field-programmable Gate Array (FPGA) – A programmable integrated circuit used to implement logical functions

Frequency Spectrum – shows the frequencies occurring from a time domain analysis, as well as the amplitudes, symbolizing the predominance of each frequency with respect to all others

Galloping Cable – A cable that can be excited via wind to structurally dangerous levels of force

Graphical User Interface (GUI) – Digital menus the user can interact with

Harmonic – A frequency that is a multiple of the fundamental frequency

Linear Ramp – A scaling factor applied to a graph proportional to the position on a specific axis

Microcontroller – An integrated circuit, run by simple functions to perform desired tasks

Natural Frequency – The frequency at which a body tends to vibrate

Nyquist Frequency – The highest frequency for which signal energies can be determined from a sample. Equal to half of the sampling frequency

Oscilloscope – an electronic test instrument that allows voltages to be viewed versus time

Peak Extraction – Determining the locations in which peaks occur in a set of data points

Radio Frequency Interference (RFI) – A disturbance that affects an electrical circuit due to either electromagnetic conduction or electromagnetic radiation emitted from an external source. The disturbance may interrupt, obstruct, or otherwise degrade or limit the effective performance of the circuit

Resonant – Self-reinforcing in vibrational amplitude

Rattling Cowbell – A device used to dissipate excess energy via making noise attached to the cable

Standing Wave – A wave characterized by a lack of vibration at certain points

Stiffness – The resistance of a body to deformation

Tension – The force per unit area exerted on a cable

Tensionometer – An instrument for measuring linear force

Problem Statement:

Instruments are to be designed that measure the natural frequency of guy wires supporting broadcasting towers to infer the cable's tension through the application of an algorithm developed by Dr. Jonathan Russell of the Coast Guard Academy. The algorithm will be enhanced by the University of Connecticut Senior Design Team and implemented in a portable laptop based system as well as a self-contained permanently installed system. The technique determines the tension of a cable by identifying the observed resonant frequencies and determining the best match within a matrix of predicted natural frequencies for the guy wire predicted at a given tension and temperature. Dr. Russell has provided code to determine the natural frequencies for a cable given its geometry and material properties. The Senior Design Team is enhancing the algorithm by automating the peak extraction and comparison processes, and building electronic systems to identify the tension automatically.

Background:

Cable tension structures are those that incorporate metallic cables under tension as structurally significant elements. Such structures include cable stay bridges, broadcasting towers, and high-voltage power lines. The cable tension of guy wires attached to antenna towers (Analog & Digital: AM / FM / TV / Loran) must be monitored periodically to ensure that cables maintain their tensile load. While likelihood of failure is low, costs of failure can be high. Failure can result in loosening of the cable, bending or twisting of the central tower or cable breakage. Such failures can damage the tower, causing loss of operation, possible human injury, and requiring replacement of the tower.

Towers are typically 1000 ft tall, ranging up to 2000ft. The central truss is formed as a triangle shaped 10ft on a side, with columns 3-6" wide of 0.5" wall tubing. Cables are strung between points on the tower and the ground in groups of three at each of several heights on the tower. These cables control the movement of the tower, rather than hold it fixed in place, and often hold on the order of 40,000 lbs tension. Full size towers incorporate heavy steel cables, inches thick, which typically sag 50 – 70ft from vertical. The fundamental (base) frequency of each cable ranges from 2Hz down to 0.2Hz (0.5 second to 5 seconds).

The current method of performing accurate cable tension measurements uses a slow, labor, personnel and equipment intensive process of attaching a coupling to each cable and physically measuring the cable tension using a hydraulic cylinder to take the load. The method generates results with 5 – 10% accuracy. This method must be repeated for each cable. Less accurate methods are used for small towers and for initial construction of larger towers. Tools that flex the cable are useful only on small diameter cables (Figure 1). One method involves line-sighting using a scope installed parallel to the cable, near the base (Figure 2). Another involves exciting a pulse in the cable and counting the cycle time for the pulse to move between the base and tower.

With any method, the center tower will require its own visual inspection to check straightness, non-twistedness, and to check bolted connections and bracket attachments. When the tower is first constructed, with the cable tensions being adjusted for the first time, this process can take weeks to accomplish. This is because the tensions of the cables must be adjusted simultaneously until the equilibrium position of the tower is attained.

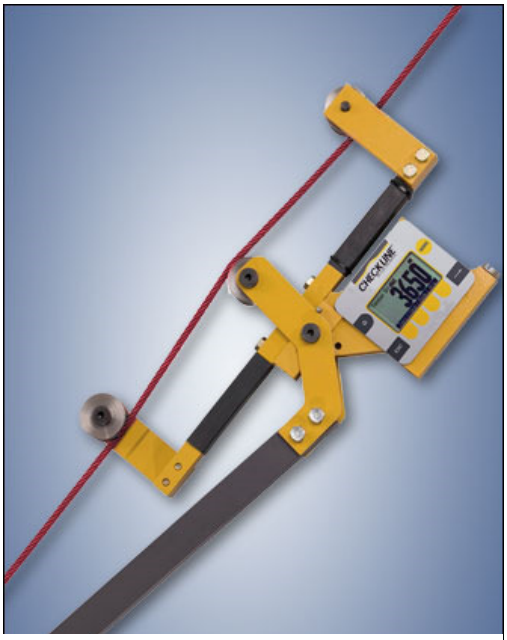

Figure 1: Small cable tension tool

Vibration techniques to determine tension in bridges are mature technologies that have been widely studied and applied. These techniques begin to fail on broadcast tower guy cables as they grow larger and incorporate significant sag and significant lumped masses at points along their length. Tower guy cables present a different problem than bridge risers, which are comparatively massive, stiff and taut. Bridge analysis techniques are accurate only for the 1st,

2nd and 3rd frequencies, not afterwards. On guy cables, these lower frequencies may have much lower amplitudes than higher frequencies, which can be used up to approximately the 20th harmonic. Furthermore, the bridge techniques do not allow for the inclusion of lumped masses along the length of the cable. The presence of significant point masses on a cable has been shown to cause banding of the natural frequencies, a significant problem to overcome when attempting vibration analysis of a system.

Figure 2: Line-sighting scope

Dr. Russell approached the Tech-Knowledge Portal Program (TKP, an EDA University Center within the Office of Technology Commercialization) with a product / business concept that should solve these problems, allowing vibration measurement techniques to be applied to large guy cables on towers. The technique uses frequency spectrum data up to the 20th harmonic of the fundamental frequency to accurately predict natural frequencies, despite the presence of lumped masses, significant sag, and inclined cable spans. After discussion with Dr. Russell, he has expressed interest in funding this as an Entrepreneurial Senior Design project. He would be interested in participating in a commercial startup business, should the project be successful.

4. Theory

This section of the report details the basic concepts behind the thesis work Dr. Russell performed on determining the tension of guy cables from their natural frequencies. Due to its complex nature, the mathematics are not detailed, but can be found in his thesis, included in the list of references near the end of this report.

Other existing vibration measurement techniques are not applicable to broadcasting tower cables, due to their unique properties. Cable sag occurs caused by the non-conducting elements placed in the cables which add a considerable amount of weight wherever they are located. Damping is insignificant in the cables and can be ignored. Vibrations due to excitement from ambient conditions including gentle breezes should be sufficient to produce meaningful measurements.

The vibration behavior of a guy cable can be compared to an elastic catenary system with negligible damping. In such a system, the cable is modeled as a stiff spring that forms a catenary shape. However, in the case of broadcasting towers, additional geometric conditions such as point loads from anti-galloping cables and point masses from non-conducting elements inserted in the cable must be considered.

Dr. Russell's core technology is an accurate method that can determine expected frequency modes on cables with significant slack and installed lumped point masses. This method is used to determine the expected natural frequencies (base frequency and harmonics) at incremental levels of tension on either side of the design (specified) tension. After a cable is measured to determine its ambient frequency response, it is compared to a matrix of expected frequencies to find the best match tension condition.(Figure 3: Flow chart of Dr. Russell's method, which uses a manual process of matching observed and expected natural frequencies

Applying Dr. Russell's algorithm determines these theoretical natural frequencies by employing finite element analysis to the system. By doing this, constraints such as the point masses can be considered on a single element as opposed to attempting to average out the mass along the cable. This allows Dr. Russell's method to predict the banding due to these point masses that occur.

By employing this finite element technique, a global stiffness matrix is generated. Dr. Russell's algorithm then uses the Newton Raphson method to simultaneously root solve for the vertical component of tension at the base of the guy cable, the horizontal component of tension at the base of the cable, and the unstrained length of the cable (if the unstrained length is not known).

Using these determined tension and unstrained length values, the algorithm then solves for the any number of natural frequencies required by the end user.

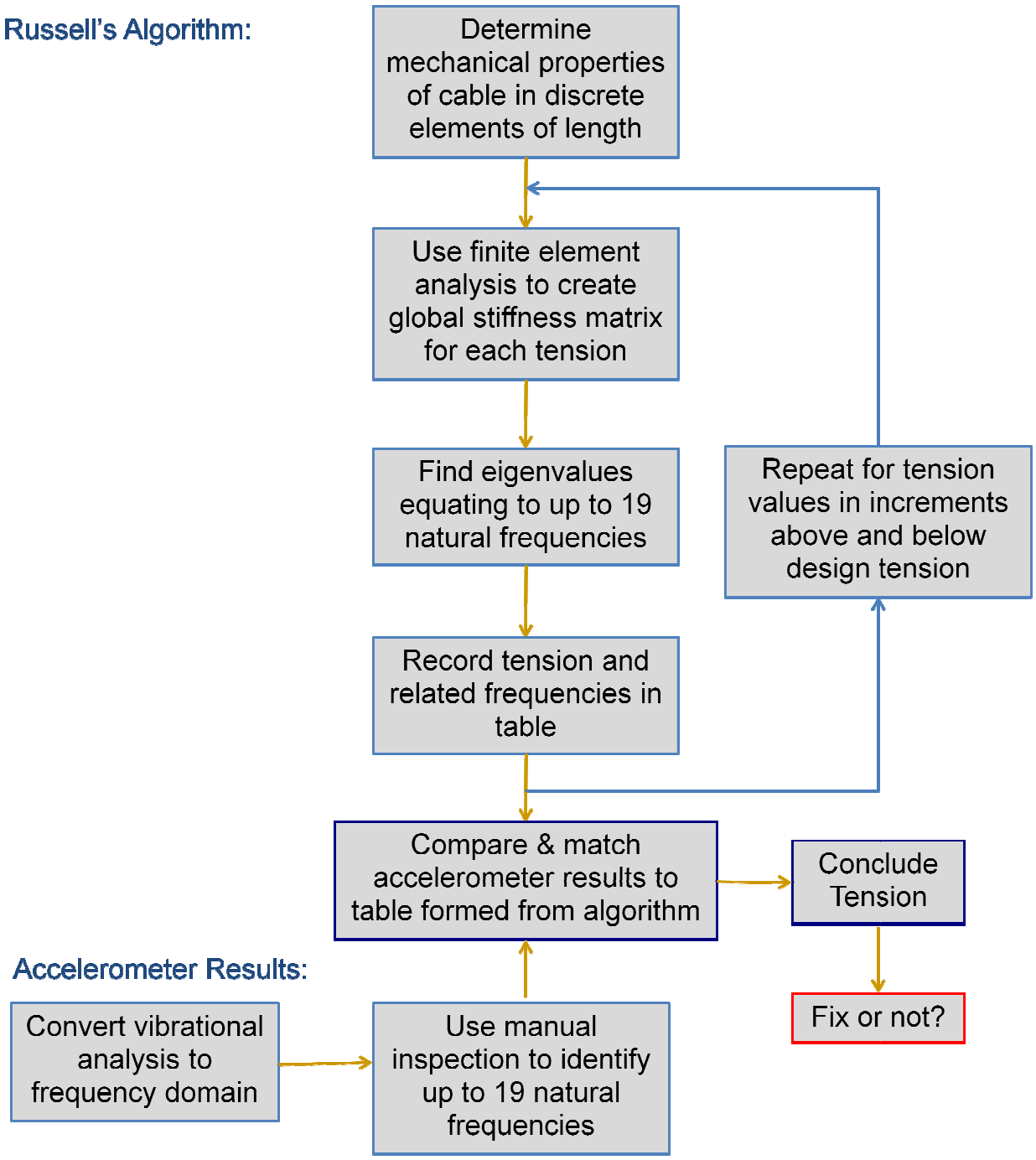

Figure 3: Flow chart of Dr. Russell's method, which uses a manual process of matching observed and expected natural frequencies

5. Approach

By implementing Dr. Russell's cable tension measuring algorithm, a smaller and more efficient portable device will be designed to monitor the cable tension. The completed device should be far more cost effective than the current process, meeting a need within the niche business of cable installation and inspection. The permanently installed version will offer continuous monitoring, not presently available in the marketplace, and may serve as a platform for additional monitoring applications.

The portable type may be temporarily attached to the cable to take a quick reading, and the collected data compared to baseline data from the original installation. This would be a fast and reliable method, and could conceivably eliminate a majority of the work associated with the currently used procedures, while delivering significant cost savings. The device would be usable by a small service team, ideally a single technician.

The permanent type could be permanently attached to a cable, performing measurements on a periodic or semi-continuous basis. Data communication could be wireless or hard-wired, and by a schedule or on-demand. The device would need to be durable under weather conditions, wear and corrosive effects, and would require a power source, which may be hard-wired, or harvest vibrational or solar energy.

The upgrade from a portable to a permanent system will allow the team to reduce costs, allow as-needed maintenance inspections, and may offer a platform for additional applications. The team will pursue both versions, beginning with the portable type to verify and refine our technique. This will be used as a test fixture to better understand the problem, refine minimum specifications and justify the design of the permanent, self-contained system. After creating an initial, working portable system, the team will swap in prototype components and build additional functionality into the working system to transition to the permanent self-contained system.

6. Design Concept

The team's design goals were to create a handheld device that can gather, store, and easily analyze data. To fulfill these needs, the team designed two separate prototypes. The first of which involved using a digital PC oscilloscope that allowed the team to gather data from our accelerometer and easily transfer the results to MATLAB for analysis. This setup was convenient because the data could be stored for repeated experimentation and interpretation as the analysis software was developed. The second prototype created made use of a digital signal processing (DSP) board to replace functionality initially performed by both the PC oscilloscope and MATLAB. This setup is more practical than the laptop-based prototype because it is smaller, faster, and can be produced cheaper.

The digital oscilloscope package that the team obtained is equipped with an automatic FFT function, to convert vibrational responses in the time domain to the frequency spectrum. The team, however, opted to collect samples in the time domain in order to implement an FFT through code to allow for an easier transition to our further design stages. The digital oscilloscope was intended for initial testing in order to verify the technique and determine minimum specifications for the digital circuit.

The digital signal processing evaluation board that the team has obtained is equipped with analog-to-digital conversion capabilities, as well as enough on-chip memory to store and analyze vibrational readings from guy cables. Data is read from the accelerometer using an on-chip A/D converter, and then stored onto the DSP's on-chip RAM. From here, the data can then be processed on the chip to perform an FFT and convert the data into the frequency domain. Once this transform has been completed, we can run our peak extraction algorithm to determine the natural frequencies occurring on the test cable. This approach has proven to retain the accuracy of the laptop-based prototype and will, ultimately, lead us to determining the tension on the cable of interest.

Laptop-Based Prototype Design

Though fully functional, and very accurate, the laptop-based prototype proved to be expensive, as well as slightly large and difficult to transport.

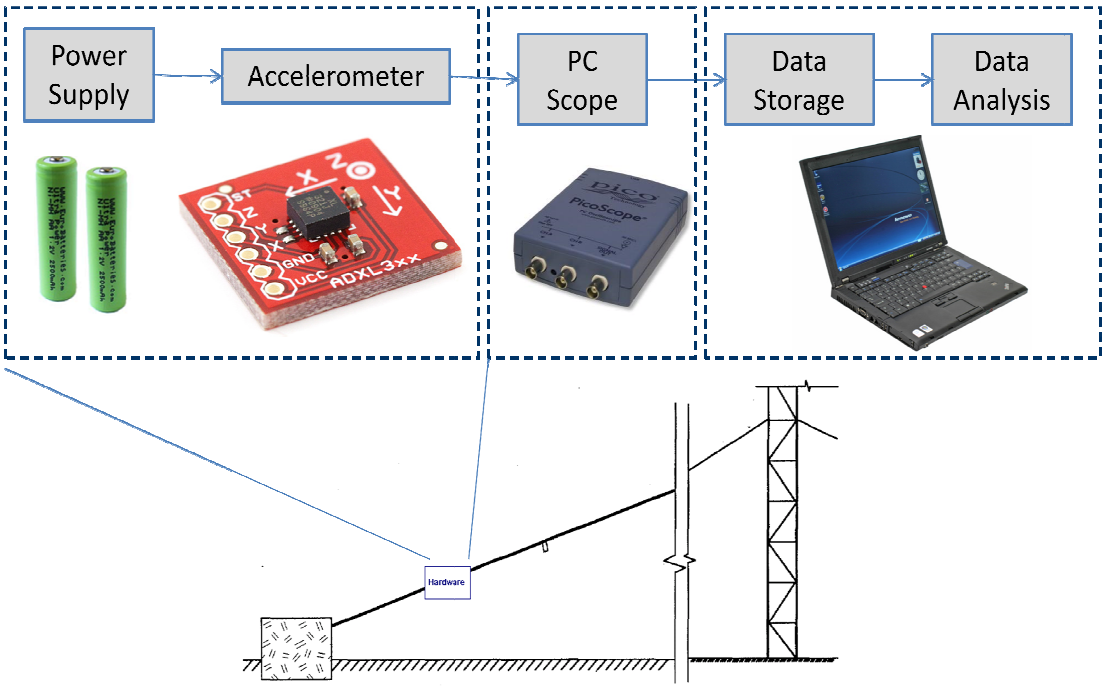

Figure 4: Laptop-based prototype hardware block diagram

Power Supply to Accelerometer

The power supply to the accelerometer must be considered separately for the portable device designs and the permanent system design. For both portable systems, the power supply itself must be portable and provide capacity beyond that necessary for a testing session. Ideally, a clean and constant signal will be provided to the accelerometer.

For our accelerometer, the power supply must be within the input limits of 2.4V – 6.0V and lacking in frequency elements within the relevant range for vibrations, 0.1Hz – 50Hz. The signal must be clean of these frequency elements, but need not maintain a consistent voltage for the accelerometer reference. The algorithm considers the frequency spectrum, while the input voltage affects only the accuracy of the signal's amplitude. These changes in amplitude are inconsequential for gradual changes induced by discharging batteries.

Batteries:

Battery Type	Pros	Cons
Disposable Alkaline	Great for convenience and initial cost.	Not ideal if you use lots of batteries. Should then consider using rechargeable batteries.
Rechargeable Alkaline	Low cost. Minimal rate of self discharge (10% per year). Shallow cycle charging bears minimal memory effects.	Short life cycle in respect to most rechargeable batteries.
Rechargeable Nickel cadmium (NiCad)	Long life cycle. Medium cost.	High rate of self discharge. High tendency to suffer from memory effects.
Rechargeable Nickel Metal Hydride (NiMH)	Medium life cycle. Low probability of suffering from memory effects.	High cost. High rate of self discharge.
Rechargeable Lithium Ion (Li-Ion)	Very long life cycle. Low rate of self discharge. Not subject to memory effects.	Very high cost.

Figure 5: Battery types

For our handheld prototypes, rechargeable NiMH batteries make the most sense. They are relatively low cost, with minimal memory effects caused by shallow charge cycling. Since an entire tower can be tested for periods within two hours, and extremely long life cycle is not necessary.

Accelerometer

The core of the vibrational measurement system is an accelerometer to convert cable motions into electrical signals for analysis. Ideally, the accelerometer should utilize communications that are EMI resistant when considering frequencies within the broadcast range(s) emitted by antennas installed on the tower. The accelerometer should be sensitive for the appropriate range of g-forces experienced by the cable, and optimally be sensitive across the complete range of relevant frequencies, 0.1Hz – 50 Hz.

EMI interference from tower broadcasts occurs at much higher frequencies (100kHz +) than the relevant cable vibrations. Digital communications may occur at these rates. The long leads for the portable system, however, may have induced signals at the broadcast frequencies. Therefore, accelerometers utilizing digital communications should be avoided. Alternatively, an accelerometer with an analog (DC) voltage will be used.

For this type of accelerometer, the DC voltage output differs from a center reference point (half of the reference voltage) by an amount proportional to the measured g-force, positive or negative. The range of g-forces experienced by the cable should remain within 0.0g – 2.0g (ambient gravity +/- 1.0g) under expected cable conditions. These values, however, may not hold under extenuating circumstances such as icing induced galloping conditions.

The low frequency response characteristics limited choices of accelerometer technologies to those that can measure DC or near-DC signals. Piezo-resistive and variable capacitance devices have this quality and were strongly considered. A leading contender piezo-electric accelerometer and an excellent match for all specifications is Measurement Specialties' 4000A model, available in several sensitivities. This accelerometer is designed for measuring long duration transients, with rated frequency response down to DC. This choice was very expensive at $335. Besides lower specified frequency handling capability, other advantages of this model such as temperature compensation are not necessary for our project. It is also very accurate, however since the team is measuring only frequencies, and not the magnitude of forces, the accuracy of the output is inconsequential.

The accelerometer chosen for the project was Analog Devices ADXL32X line. This is a close match to the ideal specifications, only missing the very low end of the rated frequency response, falling off below 0.5Hz. It is designed for sensing motion and low frequency vibrations. It incorporates a capacitance micro-sensor with a pulsed square wave applied to a silicon capacitor incorporating a suspended plate. The amplitude of the resulting signal is dependent on the relative position of the plates, and low pass filtered to produce a consistent signal. This technology is both inexpensive ($30 installed on a board and $12 for the stand alone chip) and durable, handling high-g shocks without internal damage. The bandwidth is adjusted to limit high frequency response using capacitors installed outside of the chip itself, on the breakout board. The chip includes two axis capability, however only one axis is necessary for our application. The other output is left disconnected. Our board was sourced from SparkFun Electronics and had pre-installed 1uF capacitors, which correspond to a 50Hz cut-off. The filtering will be discussed in more detail in the following section.

The initial accelerometer for the project (Analog Devices ADXL321) was sourced before fully understanding the cable behavior. A conservative choice was made to select a range of +-18g, in case vibrations exceeded +-1g from ambient. This resulted in lower sensitivity, and smaller amplitude components may have been lost below the noise floor. The accelerometer will be replaced with a more sensitive version within the same model line, the ADXL322, with a range of +-2.0g. Additionally, this accelerometer was deemed to be appropriate due to its low power consumption (340uA at 2.4V source voltage) and broad temperature range (-20°C – 70°C).

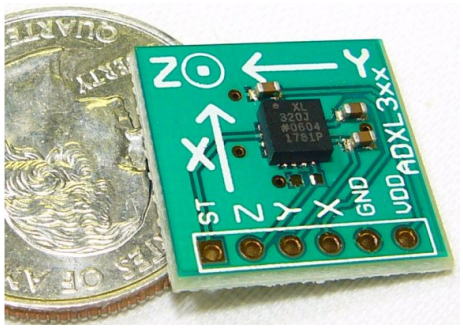

Figure 6: ADXL322 accelerometer

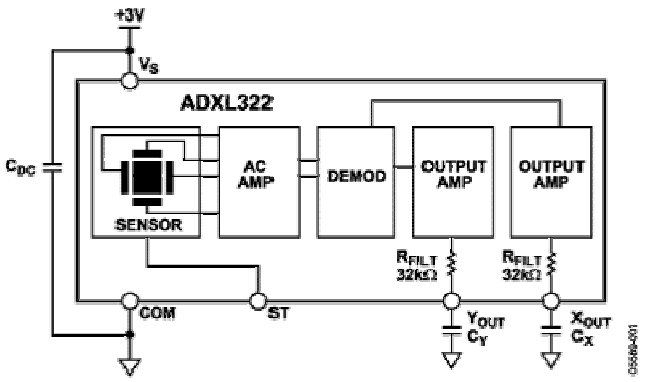

Figure 7: ADXL322 internal schematic

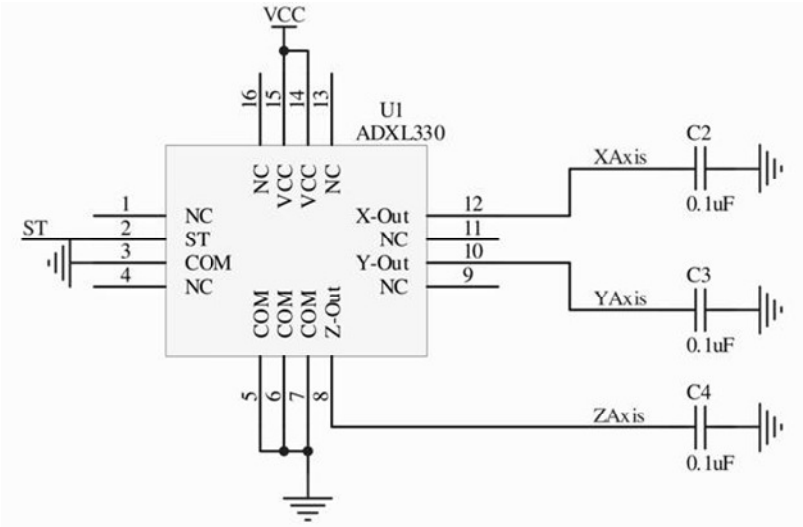

Figure 8: Accelerometer breakout board schematic

Band-Pass Filter

On the accelerometer signal output, a band pass filter is installed to reduce the effect of unwanted noise and allow the maximum resolution on the scope. The filter is composed of a low pass filter built into the accelerometer breakout board and a high pass filter at the point of the oscilloscope input. 50Hz low pass filters are included on both the X and Y axis accelerometer outputs, using on-chip 32kOhm resistors and 0.1uF capacitors surface-mounted to the breakout board. The ADXL322 accelerometer is rated down to 0.5Hz. However, it is sensitive to DC components (ambient gravity), so the rating can be considered more of an acceptable tolerance than a hard cut-off. To allow the highest resolution measurements possible using the scope, the accelerometer output was normalized to 0V average output, through the use of a 0.15Hz high pass filter. This should be close enough to the design value of 0.1Hz. This was formed by a 1uF capacitor in line with the signal output wire from the accelerometer to the scope, and the scope's own 1Mohm input resistance.

A PC oscilloscope was instituted for the laptop-based prototype in order to serve as a portable test tool for lab experiments and field-testing to verify the technique and determine the minimum specifications requirements for the embedded prototype. The scope was intended to exceed the embedded prototype needs. Picoscope's 2203 model was selected as a low cost solution that incorporated two time-matched inputs to allow for simultaneous measurements from the accelerometer and load cell during lab experiments (discussed later). The scope is portable and USB powered for relatively convenient field-testing. Data is sampled at an 8-bit native resolution, with 12-bit oversampling capabilities, and can be easily stored to a laptop to be analyzed in MATLAB. The scope can sample up to a rate of 40MHz (40,000 samples/second), but it was found that we need only to sample at around 100Hz (100 samples/second). A band-pass filter (mentioned above) was used to maximize scope resolution, and it was seen that there was typically 8 bits of variation between the scopes highest and lowest readings, as long as the system can incorporate auto-ranging capabilities. The frequency range is 0Hz – 5MHz, which more than encompasses our desired range. The scope was obtained for $245.

Figure 9: Picoscope 2203 PC oscilloscope

Embedded Prototype Design

A more unique, cost effective, and marketable design approach to monitoring the tension of guy cables. Using a digital signal processing board to replace the PC oscilloscope and laptop combination, this design provides a way to monitor tension that is much more compact, easier to transport, and requires less user interaction than the laptop-based prototype.

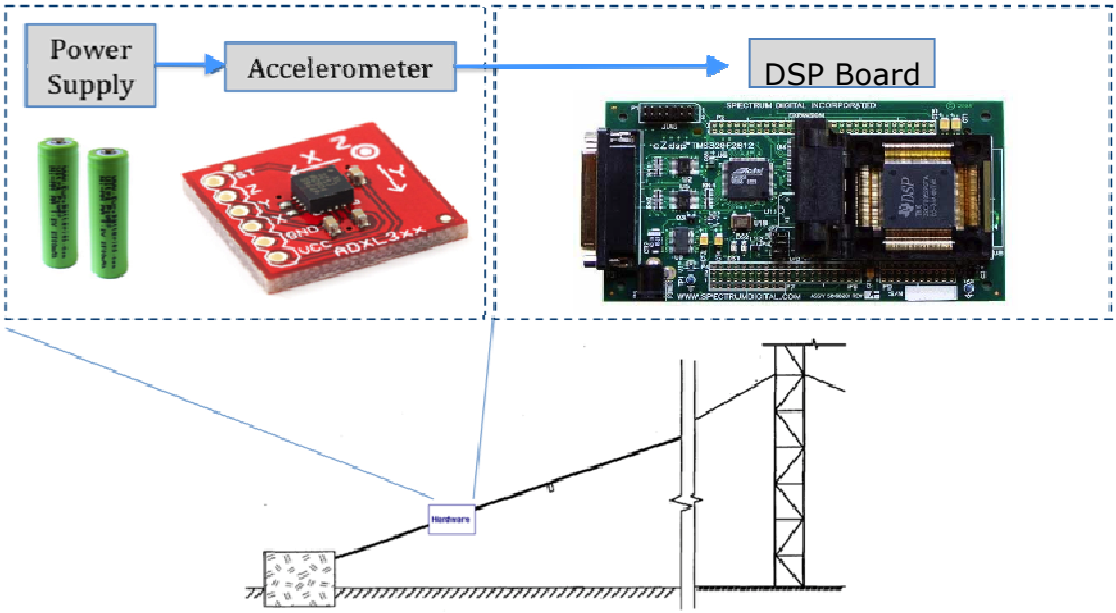

Figure 10: Embedded prototype hardware block diagram

Power Supply to DSP Board

For our DSP board, the power supply must be 5V. The signal must be clean, as well as constant. The board itself came with an AC/DC wall outlet adapter to provide 5V to the board, but we must create a portable power supply to the board in order to make our design both portable and easy to transport.

While we have yet to implement the portable power supply to the DSP board, we plan on using a voltage divider with NiMH batteries in order to provide a constant 5V. Similar to the power supply to our accelerometer, NiMH batteries make the most sense for our initial embedded design due to their low cost and minimal memory effects from shallow charge cycling.

The final embedded prototype (to be discussed later), however, will involve a fully enclosed box containing the DSP chip and its power supply. Once the team has advanced to this stage, rechargeable lithium ion batteries will be considered for the design. Although high cost, rechargeable Li-Ion batteries provide a very long life cycle, with a very low rate of self-discharge and miniscule memory effects from shallow charge cycling. These types of batteries are mostly seen in laptops, and would prove to be very effective in our final, handheld, embedded prototype.

A digital signal processing (DSP) board was implemented into our design in order to bypass the need for a PC oscilloscope and laptop combination. DSPs are geared towards the use of fast, real-time data processing. Texas Instruments' eZdsp F28335 evaluation was chosen as the best option to interface with our design. This board provides analog-digital conversion (ADC) pins as well as on board memory and up to 88 individually programmable general-purpose input/output (GPIO) pins. Additionally, the board is even more versatile for temperature ranges than our accelerometer, performing from -40°C – 85°C.

The eZdsp F28335 has a 32-bit floating point CPU and normally operates at 150MHz. The board can be run at slower clock speeds, however, in order to reduce power usage. This board is built to be a highly integrated, high-performance solution for demanding control applications such as ours.

The first of the core logic functions required by us of the DSP board is reading the voltage level outputs from the accelerometer. Our board is equipped with 16 ADC input channels, of which we only require the use of one. Each input channel performs 12-bit analog-to-digital conversions. The board's ADC has a 25MHz clock, which translates to 12,500 samples/second. This is much faster than we require, needing only 100 samples/second (100Hz sampling rate).

The next integral function required of the DSP board is storing these ADC results into the on-chip memory. The board has up to 68K bytes of on-chip RAM that we were able to utilize in storing vibrational responses from the accelerometer. Sampling at 100Hz for roughly 20 seconds, we acquire 2048 (2^11) data readings for one trial run on a cable. The data runs must be collected as a power of two in order for the FFT function to work properly. These 2048 readings correlate to about 4K bytes of data. The FFT results, which are double in size of the ADC readings, take up just over 8K bytes. Once the FFT results have been stored, the rest of the calculations and data storage required is miniscule compared to the remaining free memory space in RAM.

The programmable GPIOs on the board leave open a world of possibilities to interface analog devices. They can be set as either an input or output, and it will be later discussed as to how we can utilize these to interface such devices as switches, pushbuttons, and an LCD screen into our design. The evaluation board itself was costly at $500 (almost twice that of the PC oscilloscope), but the DSP chip itself is much cheaper at under $24. The actual DSP chip is capable of performing all functions that we utilize. The evaluation board itself was used merely for design purposes, which allowed for easy programming and debugging.

Figure 11: Texas Instruments eZdsp F28335 DSP evaluation board

Faceplate Design

To further the idea of creating a marketable product, the team looked into utilizing the DSP board's accessible GPIO pins by designing a faceplate (shown below) to encase the circuitry. This design would allow a user to easily acquire tower data, as well as visually keep track of the data analysis process. It would be ideal to implement such a design, in that it would be very simple, easy to use, and user-friendly.

With a portable power supply, the team will need a way of ensuring that the batteries are not being drained while the device is inactive. SW1 will be used as an on/off switch to place the board in a standby mode where it can power up and prepare to process data. Placed below the standby switch is a red LED indicator to show the user that the board has successfully powered on to 5V.

Once the board has been powered on, the user must input the individual parameters for the chosen cable of interest. Using the provided pushbuttons with a liquid crystal display (LCD1), a user can input the cable's unstrained length as well as vertical and horizontal spans. The pushbuttons will be designated as inputs on the GPIO pins, while the LCD will be defined as an output. From here, the peak prediction algorithm can be run – storing its results onto the DSP chip or other provided on-board memory.

Upon calculating the predicted natural frequencies, data readings can be taken from the accelerometer on the guy cable. SW2 shown below will be an illuminating, latching pushbutton switch, defined as an input, used to commence data acquisition. The purpose of an illuminating, latching switch would be so that the user can visually identify that the button has been pressed, and that it had been depressed after the previous use. Once the board senses that SW2 has been pressed, it will enter the data acquisition phase, storing the vibrational responses to the on-chip RAM.

From here on in, the user need not physically interact with the device. A series of four LED indicators are placed on the board for the user to view the stage processes of the board. LED1 indicates that data acquisition has commenced and is in progress. Once LED2 turns on, the device has begun to process the FFT function – transforming the time domain responses into the frequency domain. Status indicator LED3 symbolizes the peak extraction and comparison algorithm being run, determining the experimentally found natural frequencies and comparing them to the initially predicted resonant frequencies. Lastly, LED4 indicates that the found frequencies have been matched to those predicted, and a tension can be concluded. This final tension, as well as its condition, can then be displayed on the LCD. This way, the user can visually identify the cable's tension, as well as if the tension found can be deemed acceptable.

This faceplate design, with its analog devices, should prove to be both functionally and aesthetically pleasing to a user. The faceplate is not drawn to scale, however, as the DSP chip itself is very small – less than 2"x2" in area. Additional space will be required to provide a power supply, as well as additional off-chip memory as needed.

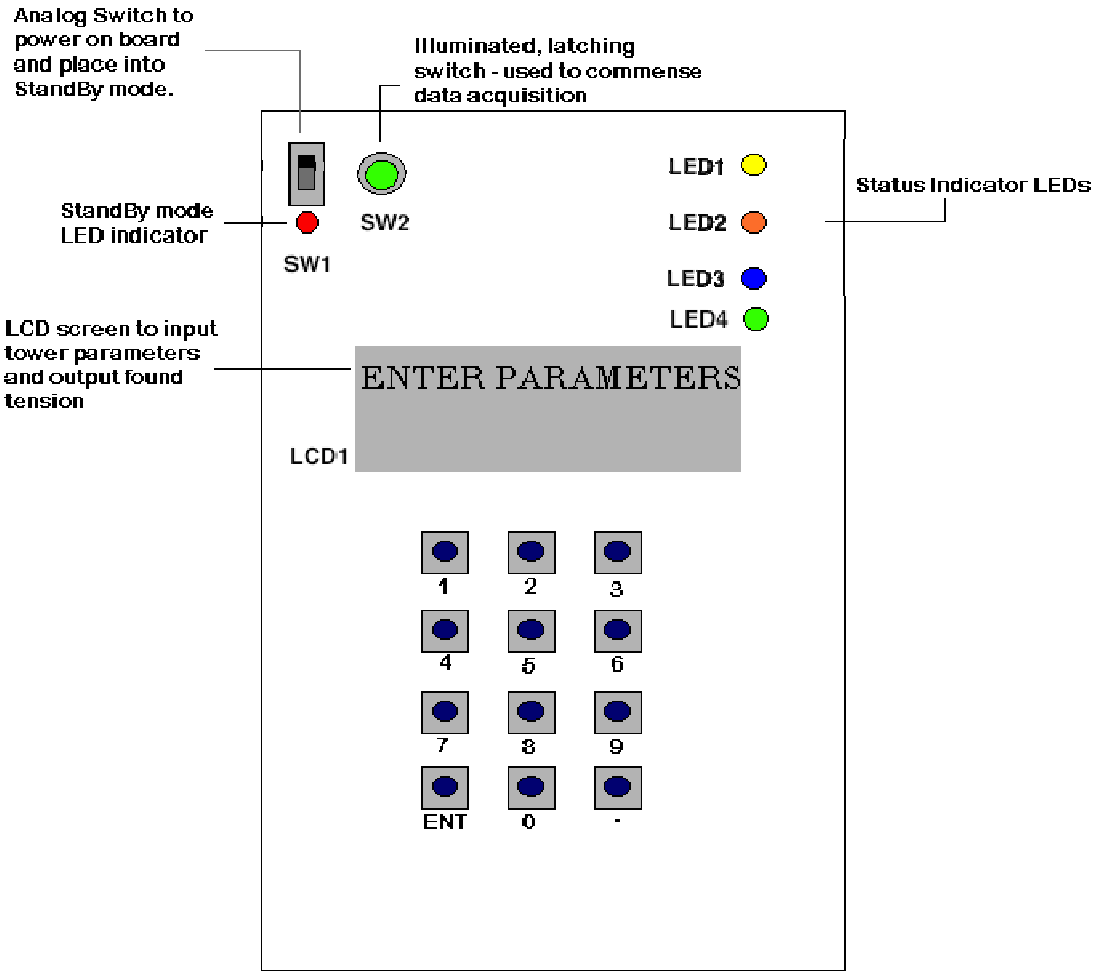

Figure 12: Initial faceplate design

Permanent Prototype

Ultimately, the team would like to design a device to be permanently installed onto guy cables for regular, off-site monitoring. Though this idea is still very much theoretical, this method would further help reduce costs by allowing many towers across the nation to be monitored all by one team from one location. This will allow for as-needed maintenance as well as further applications – such as temperature and humidity monitoring.

The first obstacle that would need to be overcome in creating a permanent prototype device is determining the appropriate power supply. The previous methods of rechargeable NiMH and Li-Ion batteries would be impractical, as the design approach is meant so that the devices will be self-operated without the need for physical user interaction. To fit our design needs, we need to explore both solar energy options as well as hard wiring to a permanent power supply at the broadcast tower's location. Solar panels would be difficult and more expensive to implement into the design, but may be necessary if certain broadcast towers do not have on-site locations for power supplies.

Upon powering the board, our device would then need to be modified from it's handheld design to reduce costs, while retaining functionality. As previously mentioned, the core functionality devices of our design can be purchased for much cheaper than we had obtained. The accelerometer chip (off-board) can be found for under $12, while the DSP chip (off-board) can be found for under $24. Additionally, with 14 ADC input channels on one DSP chip, we could essentially monitor 14 cables with a combination of 14 accelerometers and just one DSP chip. We will then be able to forgo the need for LCD screens, LEDs, and pushbuttons from the faceplate design, as there will be no need for these functionalities. Additional costs, however, will include a more durable casing intended to withstand extreme weather conditions, and a permanent installation fixture to hold the device in place. We estimate the overall cost of this design to be relatively low, with the exception of the potential need for harvesting solar energy.

In order to monitor multiple broadcast towers from a remote location, the team must then determine a proper method of transmitting and receiving results from our permanently installed devices. We can choose to analyze tower data on-site and transmit results, or we could simply transmit vibrational readings from accelerometers to be processed and analyzed at an offsite location. One precaution we must take is transmitting data is to ensure that we are not broadcasting these readings in a way that would interfere with the outputs at these broadcast towers.

This design is still very much in its early stages but seems quite tangible to accomplish in the future.

7. Concerns

Structural details and weather conditions can be problematic for a vibrational measurement system, and must be considered in our design process.

Structural:

An extra top cable made from multiple materials is often installed to adjust the electromagnetic properties of the structure. The electrical properties of the cable materials and their geometry influence the transmission characteristics of the antenna structure. One material extends from the top of the tower, an insulator is installed along the length of the cable, and the balance of the cable is made of another material. If the team attempts to incorporate the measurement of tension for these cables into the final device, it will prove problematic. However, no solution for addressing this problem is being considered at this moment as these cables are structurally insignificant.

Some towers incorporate paired cables that can be challenging for diagnosis. These are fairly rare and the team's investigation will not concern such designs. It may be possible to use vibration measurement techniques on paired cables, however this is currently beyond the scope of the project.

Components attached to the cable may affect its vibration characteristics. Installed components may include anti-galloping cables and rattling cowbells. The tower itself, if it is excited to vibrate, may drive cable vibrations.

Accurate drawings are necessary for accuracy of Dr. Russell's method as posited. It is currently unknown what the degree of accuracy necessary for the device will be as the team is currently testing the algorithm and has been unable to conduct any meaningful tests as of yet. However, it is posited that a possible solution to minimizing the effects of initial inaccuracies may be possible via measuring calculated tension change in the cable due to temperature change (possible with permanent installed device). By measuring the calculated change in tension with respect to the temperature, it may be possible to more accurately determine the unstrained length of the cable over time. However, while the team would like to pursue this possibility further, this option will only be pursued upon the successful completion of a final prototype design with a fully functional algorithm.

Furthermore, the team has not yet procured ideal data from an actual broadcasting tower. This has limited the extent to which the team can fully verify Dr. Russell's prediction algorithm.

Weather:

Weather conditions are problematic, especially when considering a permanently installed system that is expected to take measurements continuously or on demand.

Wind can cause resonant standing waves. Ice can weigh down a cable, affecting it's structural properties such that the predictions will no longer be accurate. Ice can also accumulate asymmetrically along the cable, creating an airfoil shape that may induce large amplitude galloping motions.

Lightning will regularly impact the tower and may contact the cable. While the tower and cables are constructed of conducting steel, induced voltages will need to be considered, especially near the surface of the cable. A permanent system will need to be protected from high voltage damage to the circuit through measures that may include positioning electronics away from the cable surface and shielding of the electronic component case.

The team plans to address these issues after completing a fully functional non-permanent device.

8. Data Processing

Using the laptop-based or embedded prototypes, a list of measured frequencies for the input signal is determined through a series of steps. Vibrations are first recorded for 20 seconds at 100Hz (160Hz for the laptop-based prototype). The time domain data is then transformed into the frequency domain as a power spectrum using a real valued Fast Fourier Transform (FFT) function. The spectrum is normalized using a linear ramp to equalize noise levels and peak amplitudes, so that peaks may be more readily identified across the full frequency range. A median value of noise is calculated and non-zero series of points above this value are selected. A spike function is then fitted to data at and neighboring high points within each non-zero series to accurately determine their frequencies. The following sections will explore these algorithms as well as the theory and design decisions behind them in detail.

Data Input

For the laptop-based prototype, data from the digital oscilloscope can be saved as a MATLAB file using Picoscope software. The input data is stored as an array 'A' and three variables 'Tstart', 'Tinterval', and 'Length'. The array is an n by 1 matrix consisting of voltage values sampled from the accelerometer at 160Hz. 'Tstart' provides a reference point for the entire data set and is typically '0'. 'Tinterval' represents the time between samples and varies as specified by the settings of the digital oscilloscope. For all lab data using the PC scope, the sampling rate was set at 160Hz, because the scope could not be adjusted to 100Hz. The processing algorithms were written for data at 100Hz, so raw output of these algorithms from PC scope data must be divided by 1.6 to determine actual frequency values.

The embedded prototype samples input data at 100Hz through a built in ADC port on the DSP chip that is amplitude quantized to 12 bits sensitivity over the range 0-3V. The output of the ADXL322 accelerometer is specified at 1.5V ±1.0V (or greater at maximum voltage), so the majority of the input range is used without being exceeded.

Detectable levels of noise from the accelerometer can limit the performance of data calculations. Noise could be reduced by sampling at a multiple of 100Hz and averaging multiple samples for each 0.01 second recorded data point. Data series at 160Hz recorded from the accelerometer by the PC scope were found consistent to all four decimal places recorded at 12 bits resolution, with series of or more repetitions typical for a given value during times of stability. Given this data, it seems there is nothing to be gained by averaging consecutive points.

Spectra Quality

Spectra from the lab data varied in quality as identified in qualitative visual inspections. Ratings of excellent, good, ok and terrible were determined for each spectra and color coded on the spreadsheet of input parameters and cable conditions for the 2-22 lab model data. Figure **13** to Figure **16** show examples from each category. Differences in quality did not initially seem correlated to bit width (8bit and 12 bit sensitivities where compared), input range or distortion. After more thoroughly investigating input parameters, scope settings and cable behavior, the shared qualities

of the best spectra and limitations to the data specifications became more clearly defined.

Excellent graphs are all 8 bit. Good graphs include both 8 and 12 bit. Terrible graphs are mostly 8 with one 12 bit. Excellent, good and terrible graphs occur across all input amplitude ranges from ±50mV to ±500mV. By examining the time-domain waveforms of all data samples, it became clear that all excellent spectra are at higher end of the amplitude bound. (amplitude bound refers to the maximum input value supported by the scope setting, represented graphically as the maximum on the y axis of the time-domain plot as viewed in MATLAB). The worst spectra are also at top end, but all have continually distorted waveforms. Good spectra of 12 bit resolution are found occurring range of amplitudes relative to their bounds.

The trend is that 8 bit resolution results in excellent spectra if the signal fills the amplitude range without significant distortion. 12 bit resolution results in excellent spectra even if the signal does not fill the amplitude range. Consistently overdriven signals result in terrible spectra. When processed by the peak finding algorithms to be discussed later, there was no obvious difference in performance in the number or consistency of identified frequencies between the excellent, good and ok spectra. Terrible spectra resulted in very poor performance.

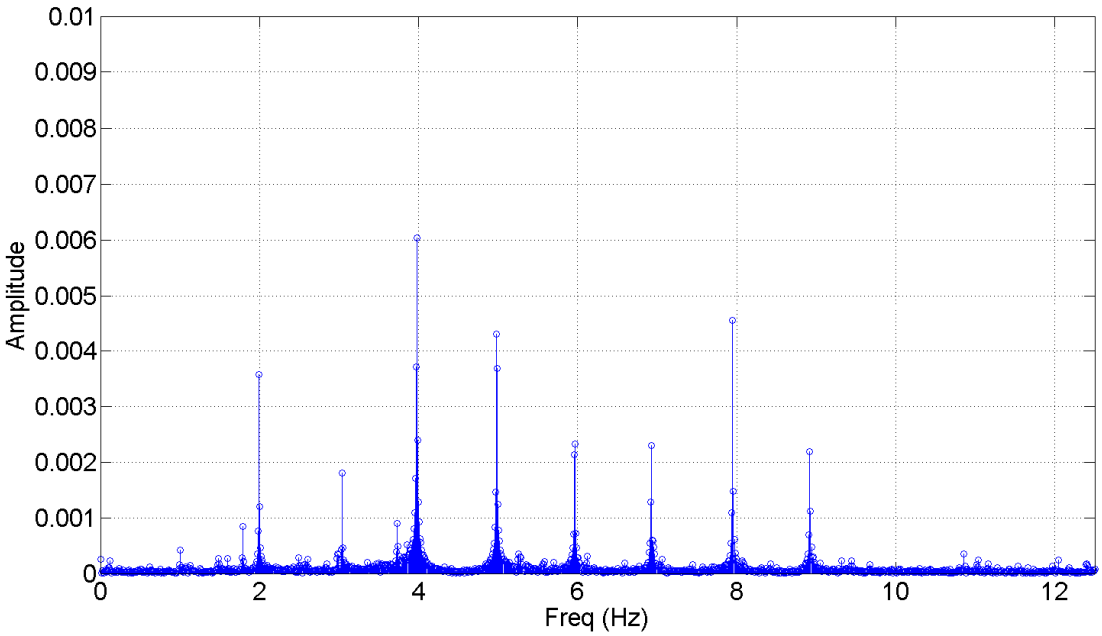

Figure 13: Run 8-2, an excellent spectrum

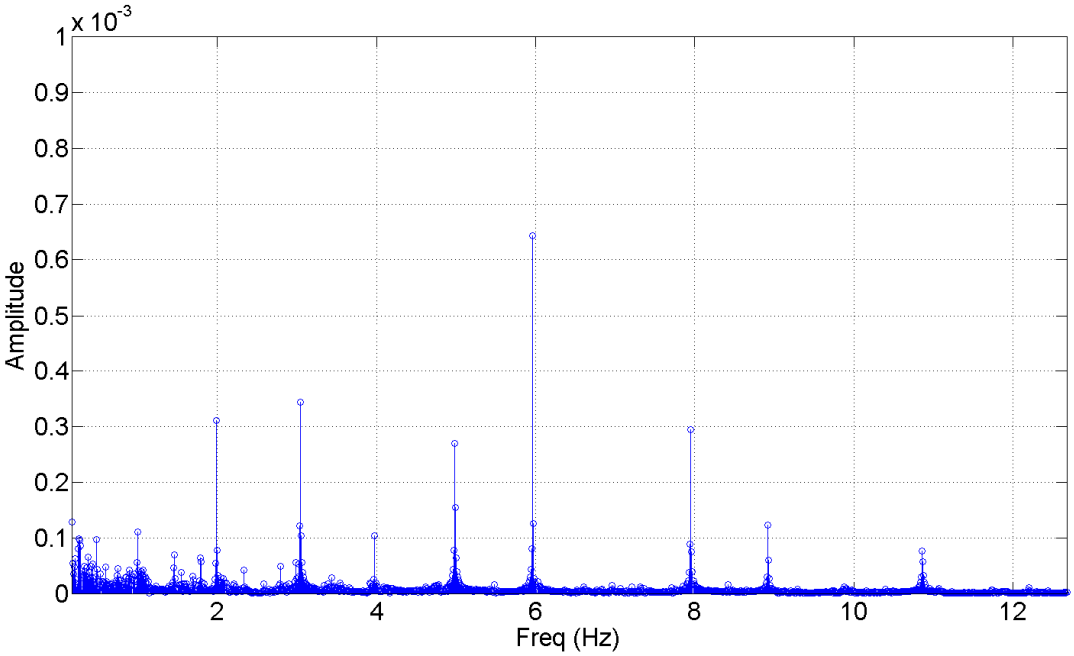

Figure 14: Run 9-1, a good spectrum

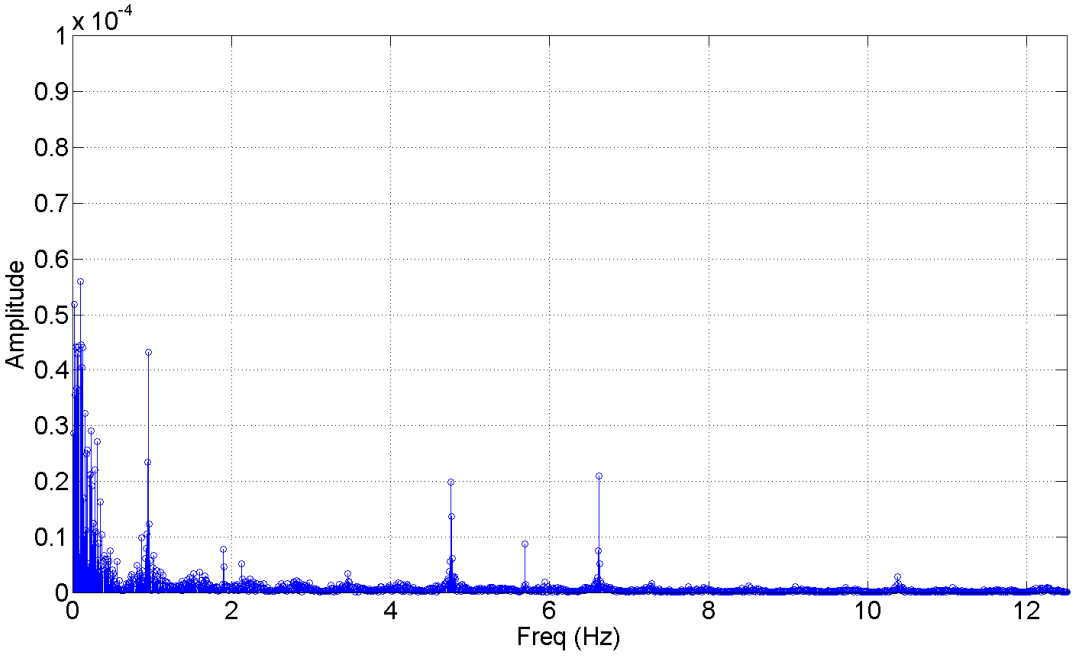

Figure 15: Run 2, an ok spectrum

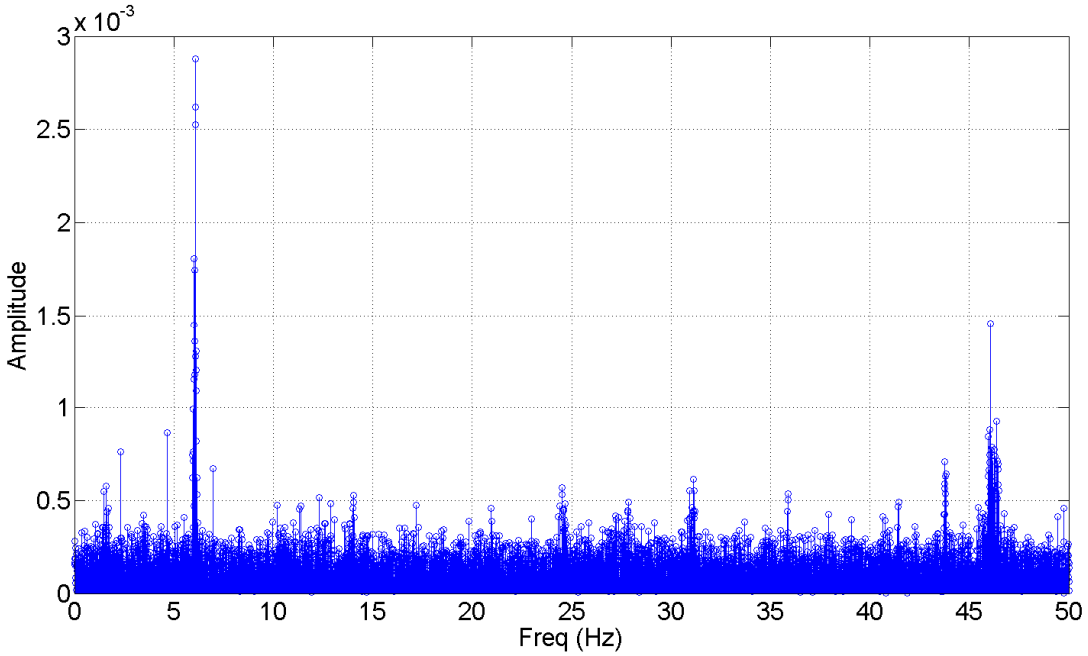

Figure 16: Run 12-1, a terrible spectrum

Amplitude Quantization

During lab testing, data was gathered at bit widths of 8 bits and 12 bits, which refer to the sensitivity of variation in sampled voltages. The discrete sampling of voltages is called 'amplitude quantization'. A bit width of 8 corresponds to 256 unique voltage divisions across the range, while 12 corresponds to 4096 unique divisions. The theory of amplitude quantization can explain the differences in performance that should be expected between different input bit widths.

The effect of amplitude quantization is equivalent to adding noise to a signal. Smaller amplitude frequency elements will not be lost unless they are lost in noise. To determine the necessary sensitivity, two questions should be answered. How much noise is already in the signal? How much noise can be tolerated in the signal? The noise is determined by the performance of the accelerometer and input circuit. The level of noise tolerated is not clearly defined. The tradeoff between noise and performance may need to be revisited if identification of additional frequencies is desired. Conversely, some noise may actually improve the effective resolution of slowly varying signals, in what is referred to as 'dithering', by alternating the signal among LSB (least-significant-bit) values that when averaged over time, offer a higher level of accuracy than individual values.[1]

[1] Smith, Steven. "The Scientist and Engineer's Guide to Digital Signal Processing." *DSPGuide.com*. California Technical Publishing, 2007. Web. April 2010. <http://www.dspguide.com/ch3/1.htm>.

Fast Fourier Transform

Time domain data sampled from the accelerometer is converted to the frequency domain using a Fast Fourier Transform (FFT) before identification and precise location of resonant frequencies.

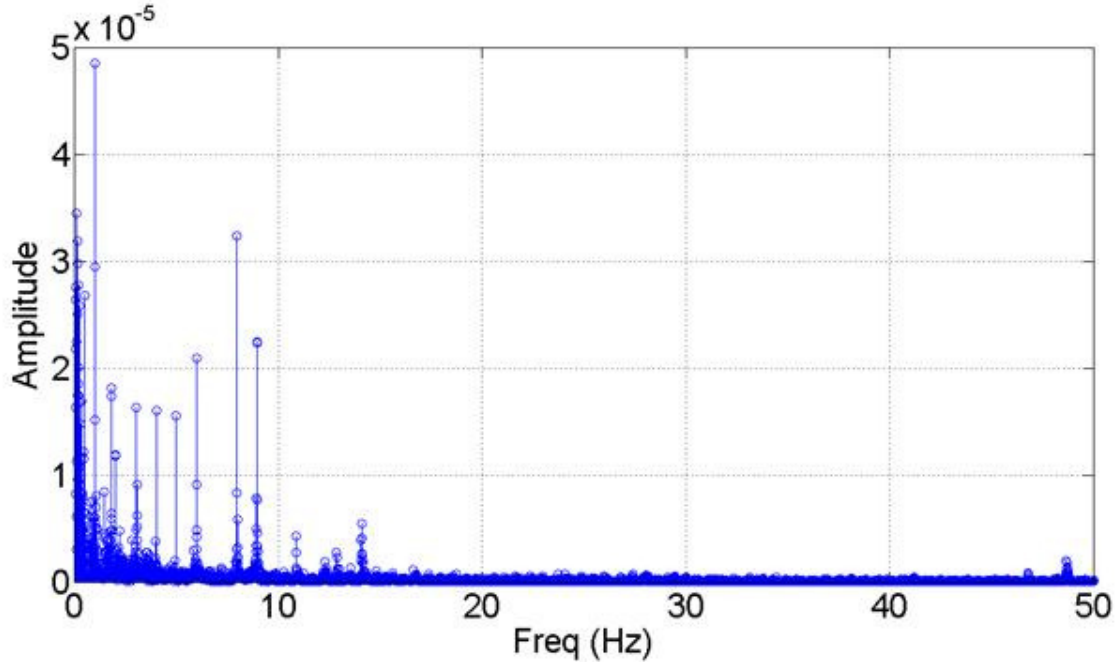

Figure 17: run 07_1 raw spectra

Figure (Figure 17) represents a typical spectrum from the lab model. A number of peaks are clearly visible between 0Hz and 15Hz. Above 15Hz, peaks are not apparent in this representation.

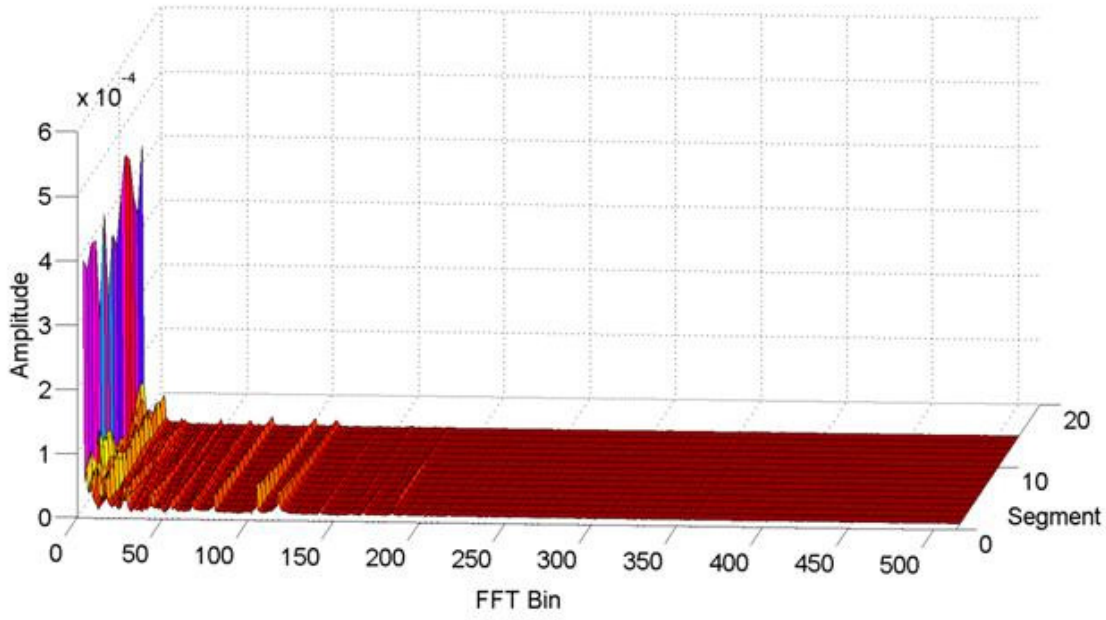

Figure 18: run 07_1, over 32 time segments

Comparing multiple spectra over time from the same run, the lower frequency peaks remain consistent and are clearly identifiable (

Figure **18**). Some faint lines at higher frequencies become visible in this representation. Between peaks, noise is more apparent towards the lower end of the spectrum, while the higher frequency end appears smooth.

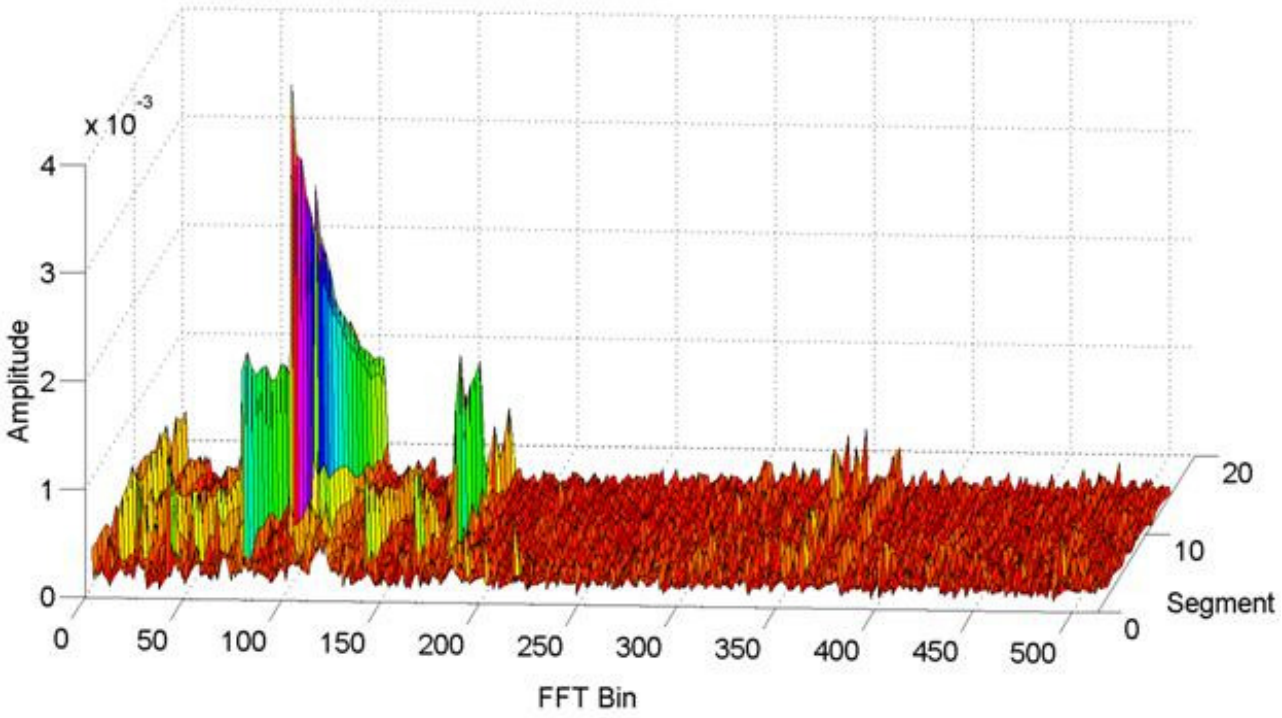

Figure 19: run 07_1 with linear ramp

After applying a linear ramp, the noise level is consistent across the spectrum from low to high frequencies and peaks are more even in height. Peaks at higher frequencies are now clearly visible.

Accuracy

The FFT function outputs a discretized series of magnitudes for frequencies up to half of the sampling frequency. The number of magnitude values in the series is equal to half of the number of samples input to the FFT function. The difference in frequency between subsequent magnitudes (a.k.a. bins) is referred to as 'bin spacing'. Higher precision (narrower bin spacing) can therefore be obtained by processing longer intervals of samples in the time domain. This precision can come at the cost of accuracy with real cable data, because tension is more likely to shift during longer test intervals due to environmental factors. A shift in tension will result in a blurred frequency spectrum, which may be less likely to result in a conclusive match.

In Dr. Russell's experience using manual inspection of traces, optimal performance for his manual identifications was obtained with measurements on the order of 30 seconds in length. To conclusively determine tension, he required 10 of 15 consecutive measurements to contain a peak frequency for that frequency to be considered for comparison to the calculated natural frequency look-up table.

To investigate the properties of the frequency spectra over time and determine optimal specifications for the peak identification algorithms, time-domain samples exceeding three minutes were taken using the lab model. These long sampling periods allowed comparison of spectra over a wide range of both sample lengths of data and starting times within the sample.

Locating Frequencies

For effective peak recognition, the frequency resolution of the FFT spectra is a critical factor. The number of bins in a spectrum is equal to half of the number of data samples input to the FFT function. More precision is desirable for peak identification, however faster performance is also desirable for a portable device and tensions can shift on real cables, which will blur spectra from longer data samples.

To explore the benefits and limitations of different sample lengths, 3D plots were generated using MATLAB to track the consistency of peaks over time, for several numbers of samples. This investigation helped determine minimum necessary recording lengths, and provided insight into magnitude differences for the same peaks in separate readings as time scales were reduced.

In this exploration, data was used from 1-14-10 lab testing, run 06, in which the cable was driven by ambient vibrations without additional excitation. The dataset has 32764 (2^{15}) consecutive samples recorded at 160Hz over 200 seconds. Earlier runs are likely affected by a cable weight that knocked against a support column. Attention is focused on frequencies between 0 and 17.5Hz. This was done before a linear ramp was considered, and frequencies above this value were not identifiable.

MATLAB functions were coded to automate the generation of multiple spectra at each timescale from the same data. The script timeSliderAdjustable.m, takes time domain input data as a one dimensional array A, and arguments numSets (the number of subsets of time-domain data to consider) and sliderFraction (the ratio of the total data length to each set data length). Using timeSliderAdjustable.m, time segments are determined with starting points evenly spaced across first half of the time domain data. Overlap occurs between time sets when slideFraction < 2*numSets. The script then selects a limited frequency range up to 24% of the total frequency range (80Hz), which equates to approx. 20Hz, to focus on valid peaks from test conditions in the run 06 data. This data is then output as a three dimensional plot. The axes include the time segment, frequency bin of the spectra, and relative amplitude of the frequency element. Amplitude units are relative and their specific value is not important.

Using the script, a plot was generated for each of 100, 25 and 6 second time segments from run 06, with numSets = 32 (Figure 20 - Figure 22). slideFraction was set at 2, 8 and 32 respectively. As longer time segments are considered, peaks are more consistent, more clearly defined, and greater in number.

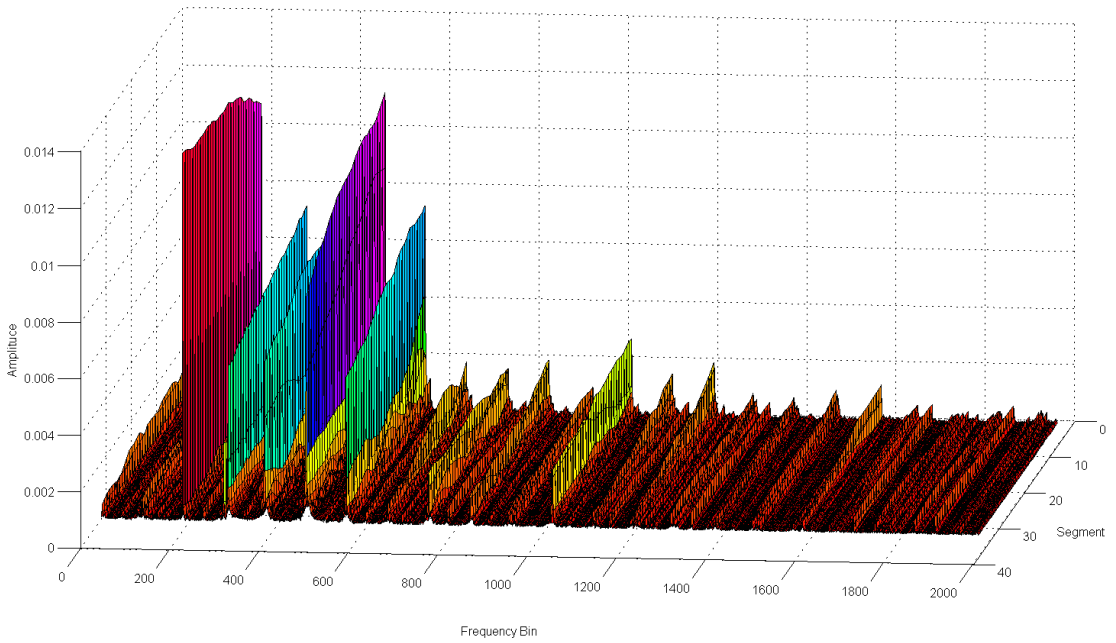

Figure 20: Time is approx 100 seconds; peaks are quite consistent across time segments.

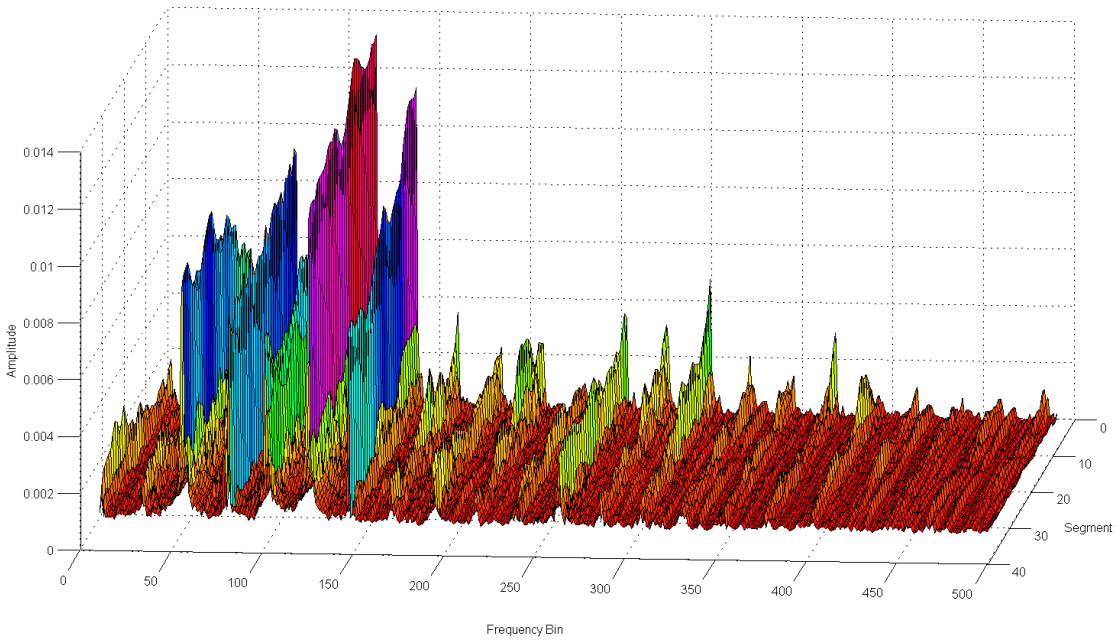

Figure 21: Time is approx 25 seconds; peaks rise and fall somewhat, but are fairly consistent

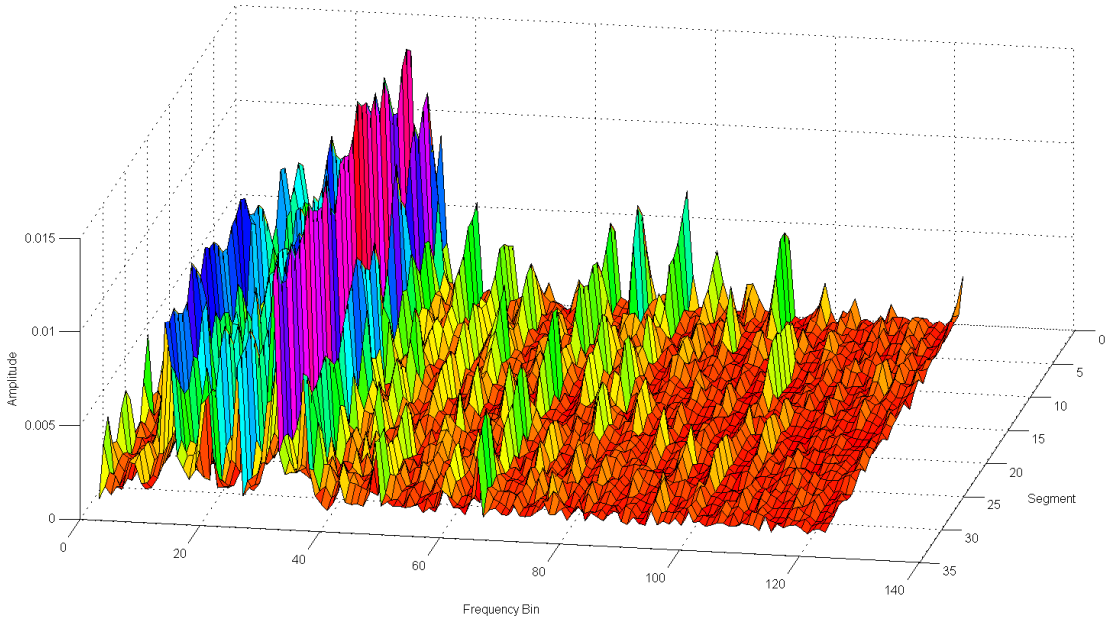

Figure 22: Time is approx 6 seconds; peaks are inconsistent, rises and falls in amplitude are exaggerated

Peak Recognition

Before peaks can be accurately identified to a high degree of precision, their locations must first be identified, so that peaks can be considered individually. Ranking the peaks by relative height versus the underlying noise had been considered, but it made more sense to use all peaks that could be found above the noise.

The final peak location algorithm was verified to have consistent performance for different tensions, input bit rates and amplitudes.

Noise Reduction

A critical element of locating peaks is elimination of noise from the spectra. After the spectra is normalized with a linear ramp, the noise is approximately even in magnitude across the entire frequency range. To focus attention on valid peaks for calculation, a magnitude cutoff level is determined above which there is little evidence of noise. Selection of this value is important. Too low, and higher noise peaks will result in false identifications. Too high, and some peaks may be too weak to be identified. All magnitude values are positive, and a simple multiplier was chosen experimentally to eliminate the vast majority of noise, while preserving as many peaks as possible. The median of all spectra magnitudes was first calculated. The product of this value with a constant determined the noise cutoff level. Using a mean had been considered, but the median should better represent the height of the noise, without undue influence from tall peak points. Spectra from 2048 samples was processed with multipliers between 1 and 4. These first considered only consecutive series of values above the cutoff point.

Figure 23: 07_1 & 07_2 at 12 sec Peak 1x median

Figure 24: runs 07_1 & 07_2 at 12 sec, 1.5 x median

Figure 25: runs 07_1 & 07_2 at 12 sec, 2x median

The criteria of consecutive values eliminated a number of consistent peaks that were large in magnitude, but too narrow to contain more than one bin value above the noise. Removing this 'consecutive criteria' included these peaks, and more frequencies were identified.

Figure 26: runs 07_1 & 07_2 at 12 sec, 1x median; no consecutive requirement

Figure 27: runs 07_1 & 07_2 at 12 sec, 1.5x median; no consecutive requirement

Figure 28: runs 07_1 & 07_2 at 12 sec, 2x median; no consecutive requirement

Figure 29: runs 07_1 & 07_2 at 12 sec, 3x median; no consecutive requirement

Figure 30: runs 07_1 & 07_2 at 12 sec, 4x median; no consecutive requirement

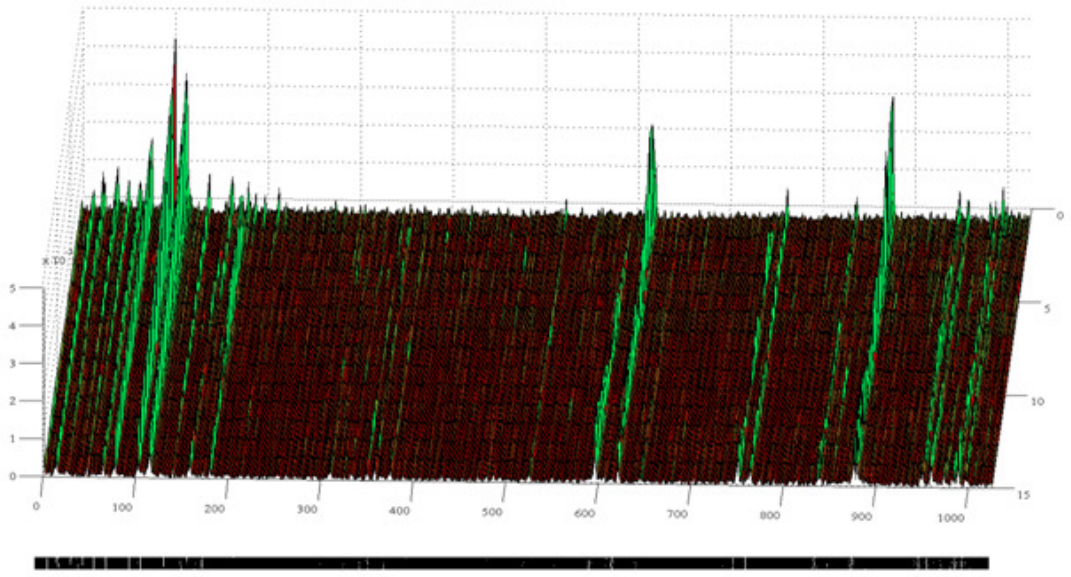

Figure 31: peaks represented over time in spectra (above) and as located (below)

The final peak location algorithm consistently identifies frequencies within one bin spacing for different tensions and bit rates. Its performance is consistent for amplitudes with a minimum of 8 bits of variability and not continually distorted.

Peak Fitting

While peak location using high bins within the spectra offered consistency of identification, higher accuracy could be obtained using fewer samples and / or less time by implementing an effective fitting function on the peak high point and its neighbors. The frequency identification accuracy before fitting is equal to the spectra bin spacing. At 2048 samples taken at 100Hz, the FFT bin spacing is +-0.05Hz.

Curve Fitting

Least squares curve fitting was initially considered to identify peaks within each spectrum to more accurately identify resonant frequencies. This method approximates the curve shape with a polynomial function and determines peak locations from downward zero-crossings in the first derivative. This method is more useful for signals that have several data points in each peak, and less useful for signals exhibiting narrow spikes comprised of only one or two points.

To avoid undue influence of noise elements, a second order polynomial regression fit was investigated. A parabola was fit the highest bin and its nearest neighbor on each side. The roots of the parabola were calculated, with the peak frequency determined from the midpoint between roots. This method was implemented in MATLAB using multiple functions.

squareReg.m: 2nd order regression on three points (at relative bin values -1, 0, 1) to determine parabola coefficients.

quadForm.m: Determination of roots from coefficients.

peakOffset.m: Uses squareReg.m and quadForm.m to find peak point at midpoint of roots.

curve3FindPeakOffsets.m: Given the spectra size, spectra and list of bin locations for found peaks, use peakOffset.m to locate each peak using curve fitting and form a list of peaks.

processLCurve3.m: Complete processing of 1 segment with a specified number of samples using 2nd order poly curve fitting to generate peak list.

processSCurve3.m: Complete processing of a numbered consecutive segment with a fixed number of samples using 2nd order poly curve fitting to generate peak list.

Using the method, frequency lists were calculated for increasing lengths of samples (powers of 2 from 512 to 8192) and for seven consecutive time segments of equal length. When comparing increasing lengths or consecutive segments, frequency identification was consistent for many frequencies to within approximately .005Hz.

Spike Fitting

With the tall, narrow shape of most peaks, there is often not more than one element on each side of the highest point before the signal is amongst the noise. Given this shape, a spike seems a more natural fit to the frequency domain peaks. A parabola's downward curve does not match the asymptotic steep approach to the high point, while there are often not enough elements on either side to gain much value from a Gaussian curve fit.

To define the spike, the largest equilateral triangle possible was fit underneath the high point and one neighboring point from the frequency bin on either side. First, a line is fit between highest and lowest points of these 3 points. A line of opposite slope is then fit to the middle point. The intersection of these two lines defines the horizontal coordinate of the identified peak, and the offset from the high point is determined in units of bin spacing for simplicity of calculation. Such a triangle looks to be a good approximation of the asymptotic spike appearance of the peaks and is computationally efficient to calculate.

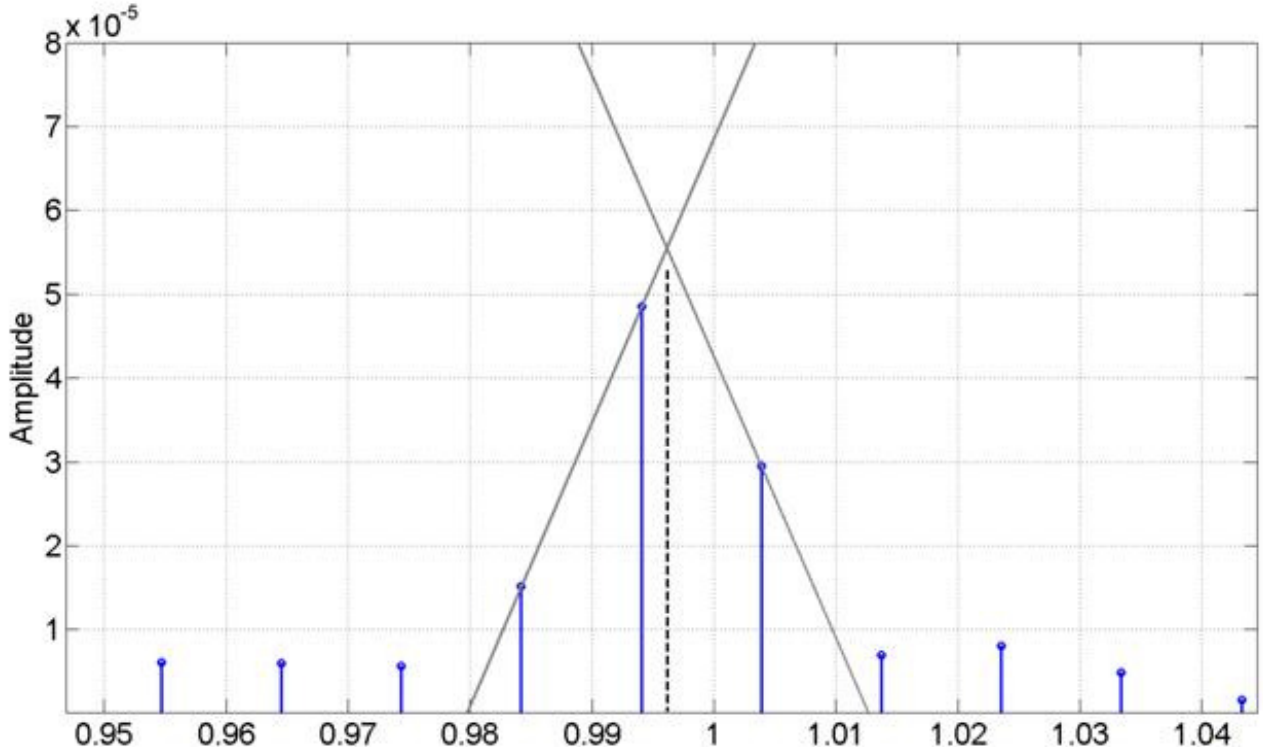

Figure 32: illustration of spike fitting process

This method was verified by hand on a few peaks from Run 07_1 spectra from the 2-22-10 lab data. The fit of the method looks quite good, finding peaks near the high point when symmetrical and near the center of 2 high points when middle point is close to high point. For two taller peaks with more neighbors forming the approach curve, the spike method was performed using the 1st, 3rd and 5th of the high point and its four neighbors for comparison. The intersections found were the same. A combination of three points was used for the implementation as coded in peakSpikeOffset.m. Further investigation may determine if a combined method using five points can offer greater precision. If five points are used, the proximity to the noise cutoff should be considered, and more weight given to the three point intersection.

$$\frac{y - y_1}{x - x_1} = \frac{y_2 - y_1}{x_2 - x_1}$$

Figure 33: Line from first and lowest point to high point

$$\frac{y_1 - y_2}{x_2 - x_1} = \frac{y - y_3}{x - x_3}$$

Figure 34: Line with opposite slope through third (middle height) point

$$x = \frac{x_3 + x_1}{2} + \frac{y_3 - y_1}{2}\left(\frac{x_2 - x_1}{y_2 - y_1}\right)$$

Figure 35: X coordinate of spike peak

$$x_1 = -1, x_2 = 0, x_3 = 1 \quad \therefore \quad x = \frac{1}{2}\left(\frac{y_3 - y_1}{y_2 - y_1}\right)$$

Figure 36: Peak offset relative to bin spacing (when 1st point is lowest)

The spike fitting method compares favorably with the parabolic curve fit, offering similar precision. Using the spike fit within the MATLAB algorithm, increasing lengths (processLSpike3.m for lengths 512 to 8192) were considered and variances determined between identified frequencies from the different input lengths. Variances are almost identical (only slightly worse on average). The average among frequencies of variance between IDs at different lengths was 0.01682 for parabola fit and 0.01687 for the spike fit. Next, consecutive, independent segments of 2048 samples were considered and results compared to those from the parabola fit. The average difference in the spike versus parabola fit was approximately ±.0022Hz, or 4.4% of the .05Hz bin spacing. Given the similar results level of consistency between methods, the spike fit was chosen for more efficient computation.

Coding

Before porting to C, the MATLAB code was first divided into smaller, cohesive functions and optimized for efficiency with a focus on generation of values through the core algorithm, rather than data visualization.

MATLAB's embedded hints tag '%#eml' aided coding for efficiency by highlighting where variables could be pre-allocated and loops simplified.

MATLAB is very flexible regarding variable typing, but often not memory and speed optimized. For the transition to C, it was important that variable types are efficient for C (MATLAB may default to 64 bit values). Also, array indexes needed to be adjusted to begin at 0 on C versus 1 on MATLAB. This required adjustment of a number of parameters and equations.

(See appendixes for MATLAB processing code and embedded C code)

Fast Fourier Transform

A key strength of the DSP board as a foundation for the embedded prototype is the set of hardware signal processing blocks that offer fast and efficient computations for commonly used functions including FFT. Use of these blocks required installation of related libraries and header files on Code Composer Studio, so that they could be called from functions.

There were three FFT functions available for consideration:

RFFT_f32: includes input bit reversing, requires input buffer alignment.

RFFT_f32u: includes input bit reversing, does not require input buffer alignment,

somewhat lower performance.

RFFT_f32_mag: computes real FFT magnitude (matches common math software),

uses output from either above function.

RFFT_f32_mag was chosen and was implemented with RFFT_f32u as a foundation. This is not the most power or time efficient FFT implementation, but it offers simplicity in design and debugging and requires less memory space. A more streamlined implementation using RFFT_f32 may be worthwhile for future implementations that require battery power or have more constrained speed requirements.

Memory Management

Memory management was a critical and challenging area of attention when adapting the C code to target the Ti DSP. With several large arrays combined in the on-chip SARAM memory, array variables needed to be carefully declared and pre-allocated to prevent overlapping memory addresses and overwritten values. Contention for memory locations did not result in failed compilation or errors, but was discovered during debugging. To fix these problems, the critical arrays were declared before main() as global variables to ensure memory allocation. The memory map of the DSP was then adjusted to fit components into RAM locations.

Verification between MATLAB and embedded C on the DSP

Two methods were pursued to test the DSP implementation of the MATLAB code. First, the ADC on the DSP was used to record input data which was then copied to Excel from the debugger and imported into MATLAB. A known frequency sine wave from a signal generator was tested and the identified frequency matched the generated value. Next, MATLAB data from lab testing and the Waterford tower was exported to Excel and adjusted to match the unsigned 16 bit integer format of the DSP time-domain array. The array was initialized in C code to these values and the ADC was disabled, so that these values would be processed by the system as if they had been recorded directly by the ADC. This facilitated debugging, by allowing direct comparison to MATLAB intermediate computations. After concluding debugging, the system has been confirmed to generate the same peak list values as the proven MATLAB algorithm.

Tension Look-up Table

Dr. Russell's existing method of frequency matching is based on human pattern recognition and intuition in determining a match. Dr. Russell's claimed accuracy is within 1%, which is superior to measuring requirements of 5% tolerance.

To fully automate tension determination from time-domain data, a confidence score must be determined for each possible match between the list of found frequencies and the list of predicted frequencies. Determining such a score is challenging for a number of reasons. Some frequencies will be found that are not predicted, and many frequencies may be predicted but not found. Frequencies that should be considered a match will match within a range of values, due to granularity of the look-up table tension increments and errors in frequency prediction due to geometric measurement errors or model limitations.

Some properties of the table look-up algorithm have been specified, but design and vetting of a specific algorithm is dependent on additional laboratory data with a range of tensions known to a high level of accuracy. These ideas have not been tested.

For each found frequency, close matches to frequencies from lookup table are first identified. Considering the number of matching frequencies alone is problematic, because more than one tension may be identified with differing numbers of matches. The likelihood of false positive tension identifications will need to be reduced to an acceptably small level.

To determine the tolerance for lookup table comparison, results were taken from the highest bin location algorithm for peak recognition (without curve or spike fitting and with sample length 25.6sec, OverNum multiplier of 4, no consecutive criteria, limited to 10 most consistently identified frequencies under 30Hz). 38 differences between each frequency and the next higher frequency from the same peak ID result were compared to determine the minimum spacing in Hz between identified frequencies. 33/38 (87%) of differences are over 20 bins (0.8Hz). 36/38 (95%) of differences are over 16 bins (0.64Hz). This spacing matches Dr. Russell's journal results (Figure 37), in which most frequency differences are greater than or equal to 0.8Hz. The maximum window for considering a match should be half of the minimum common difference, which is 0.32Hz. This spacing is problematic for some lower frequency modes that closely approach one another due to avoided crossings. A narrower window for matching, ignoring duplicate matches, or allowing duplicate matches should be considered.

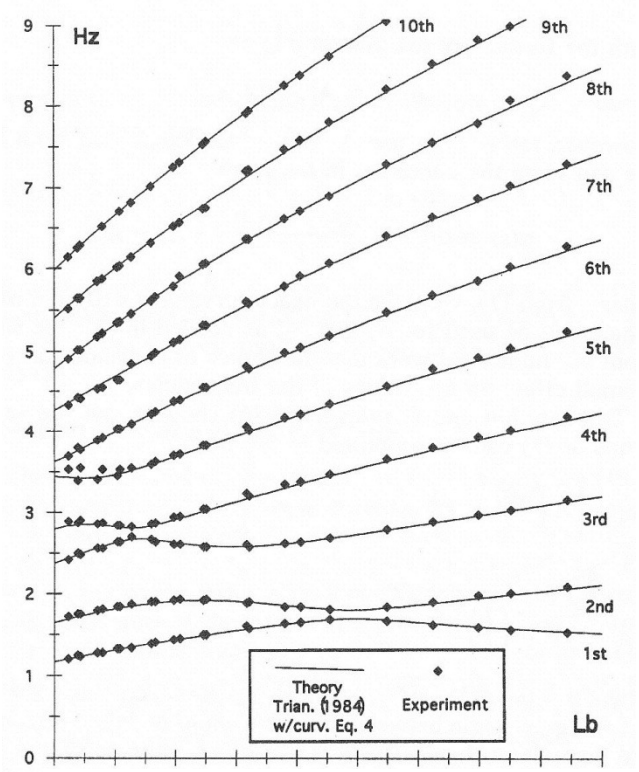

Figure 37: Natural Freq. vs. Base Tension

Two factors should be weighed to determine the confidence of a match to an identified tension. First, the number of found frequencies matching will give a general score to the match. The window should be wide enough to identify most likely candidates. This width is dependent on the increments of tension in the look-up table, as well as the levels of uncertainty in frequency identification and modeling. Uncertainties may not be constant for different frequencies, depending on equipment and cable characteristics. Conversely, narrower windows should offer less false positive identification. A window of ±0.08Hz to ±0.16Hz (5 to 10 bins) is suggested to accommodate the fluctuations observed in identifications from lab model measurements.

The second factor to determine the match confidence is the differences among matching frequencies between the found and predicted values. To gain a higher level of accuracy in identification, frequencies in between look-up table entries can be interpolated to minimize these variances. Because of the incidence of frequency elements not predicted, the algorithm should give more positive weight in match confidence to close matches than negative weight to distant matches.

Given a tale of predicted frequencies for base forces from 22lb to 43lb, three peak series from the 2-22-10 data were compared. This data included corresponding relative force measurements, but not specific force values, because the load cell had not been calibrated. Frequencies from first run 07_01 (5700 force) did not match, and appeared related in spacing and value, but consistency lower than 22lb predicted

frequencies. Higher force value runs with acceptable spectra were necessary, so frequency lists from runs 10 (9175 force) and 13 (9550 force) were matched to a table of predictions with 0.8lb spacing. Run 13 matched 5 frequencies within 0.03Hz to 33.77lb predictions (Figure 38), while run 10 matched 3 within 0.03Hz to 31.01lb predictions with 3 more matches to frequencies predicted at neighboring force values. The matching frequencies for both runs were in the range of 2Hz to 6Hz. No other look-up table forces offered more than one or two close predictions for the measured frequencies for these runs. The ratio of measured tension between runs 13 to 10 was 9550/9175 = 1.04, which is close to the ratio of the matching force values 33.77/31.01 = 1.09. The difference between 1.04 and 1.09 is well within the error of the tensionometer measurement and spacing between look-up table forces.

Predicted	2.46	3.67	4.84	6.02	24.21
Found	2.46	3.68	4.86	5.99	24.23
Difference	0.00	0.02	0.02	-0.03	0.02

Found, not predicted	Predicted, not found
4.69, 7.20, 8.42, 13.98, 23.59	1.41, 6.95, 10.29, 10.77, 11.65, 12.66, 13.66, 14.55, 15.24, 20.48, 20.97, 21.48, 22.22, 22.99, 23.67

Figure 38: Run 13 predicted frequency matches

Frequency Relationships

To understand the information content of sets of identified frequencies, it is important to understand the relationships among them. Identified frequencies with linear relationships between different tensions represent less information than the same number of unrelated frequencies. Constant frequencies may be related to external forces, rather than the cable properties. Data from the 2-22-10 lab sessions was searched for linear and constant relationships.

Given each tension and list of identified frequencies, the predicted frequency values at the other tension values were calculated using linear scaling. There were a minority of points that had possible linear relationships and fewer possible constant relationships. It is not conclusive whether there is any relationship. Within a set of 8 frequencies in another list, two and maybe three were possibly harmonically related.

Another interesting relationship became apparent during lab testing. Without any other adjustments, when the cable was oscillating at higher amplitude, a higher tension was reported on the tensionometer. These differences were not noticeable from the found frequencies over time as the oscillations faded away.

Consistency of Frequency Identification

Ideally, the same frequencies should be identified given any arbitrary starting time for a cable under the same conditions. The level of consistency in identification is important when considering the window of consideration for matching predictions to found frequencies and the level of confidence that can be inferred from the variance between these values.

Between consecutive, separate time segments of 2048 samples, identified frequencies using fitting were consistent within only about 0.05Hz, equivalent to the bin spacing of the FFT function. To understand these fluctuations, frequencies were predicted for a 2048 sample sliding window of time across data. Between iterations of the peak identification algorithm, the starting time was incremented in 100, 10 and 1 sample increments to track shifts in identified values. To automate this process and provide coherent output, a MATLAB function peakTracker.m was implemented. The input data, number of samples to consider for each iteration, increment (stride) of subsequent runs, and a minimum percentage of occurrences for a given 0.1Hz window is input to the function. The function automatically organizes the found frequencies into columns of frequencies within 0.1Hz windows, so that trends may be easily plotted and identified.

Using the peaktracker.m function on data from run 07_1 from 2-22-10, the algorithm was set for 2048 sample segments with a minimum frequency occurrence of 75%. 12 frequencies were consistently identified across starting times. Frequency identifications within each window appeared randomly distributed above 10 sample increments. At and below 10 sample increments (equivalent to 0.1 seconds or 0.01 seconds), distinct sine wave patterns were clearly visible as seen in the following figures. These oscillations occur in all frequency windows, but do not appear related between windows. Oscillations are equivalent in Hz between high and low frequencies. This means that oscillations relative the frequency value are much greater for lower frequency than for higher frequencies. Compared to the maximum value for each window, the lowest frequencies oscillate up to about -3%, while the highest 2 frequencies oscillate up to about -0.1%.

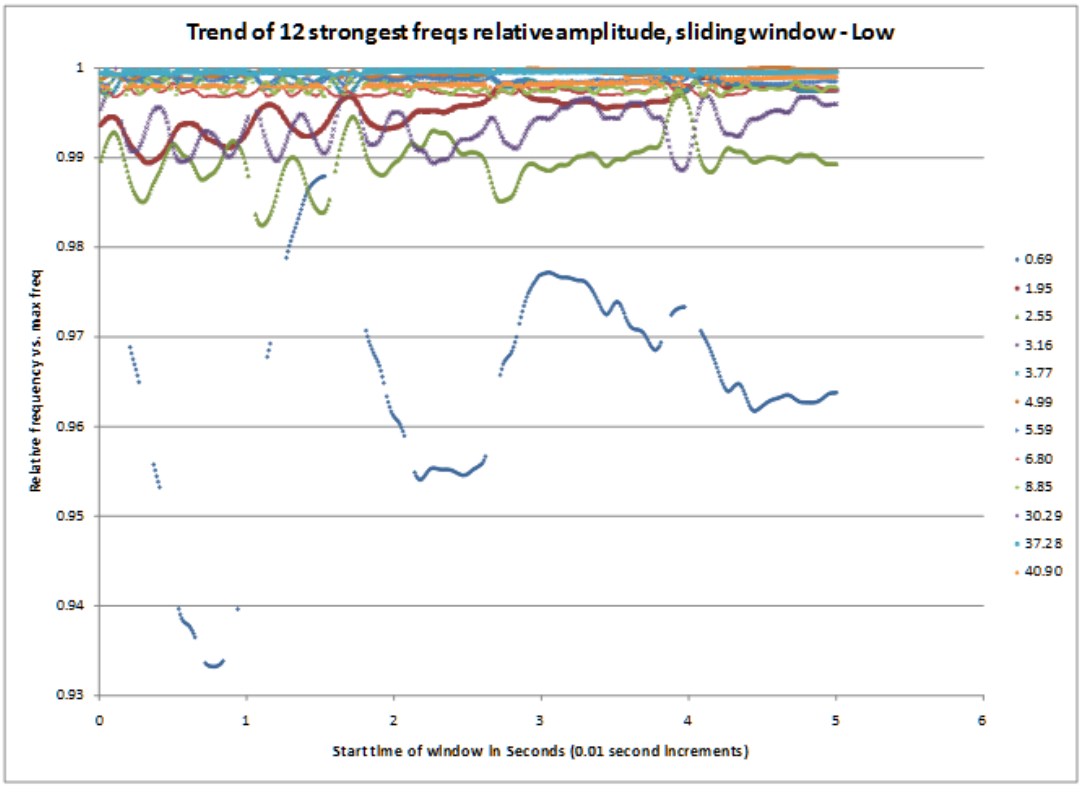

Figure 39: trend of low frequencies over 5 seconds

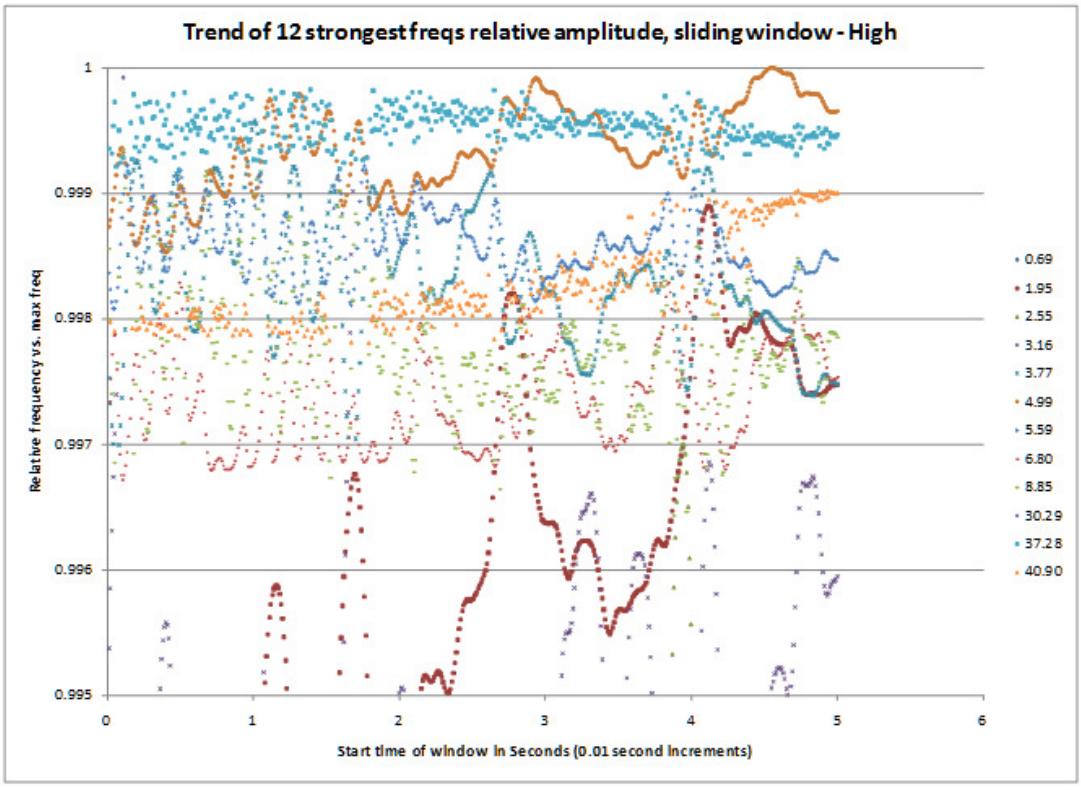

Figure 40: trend of high frequencies of 5 seconds

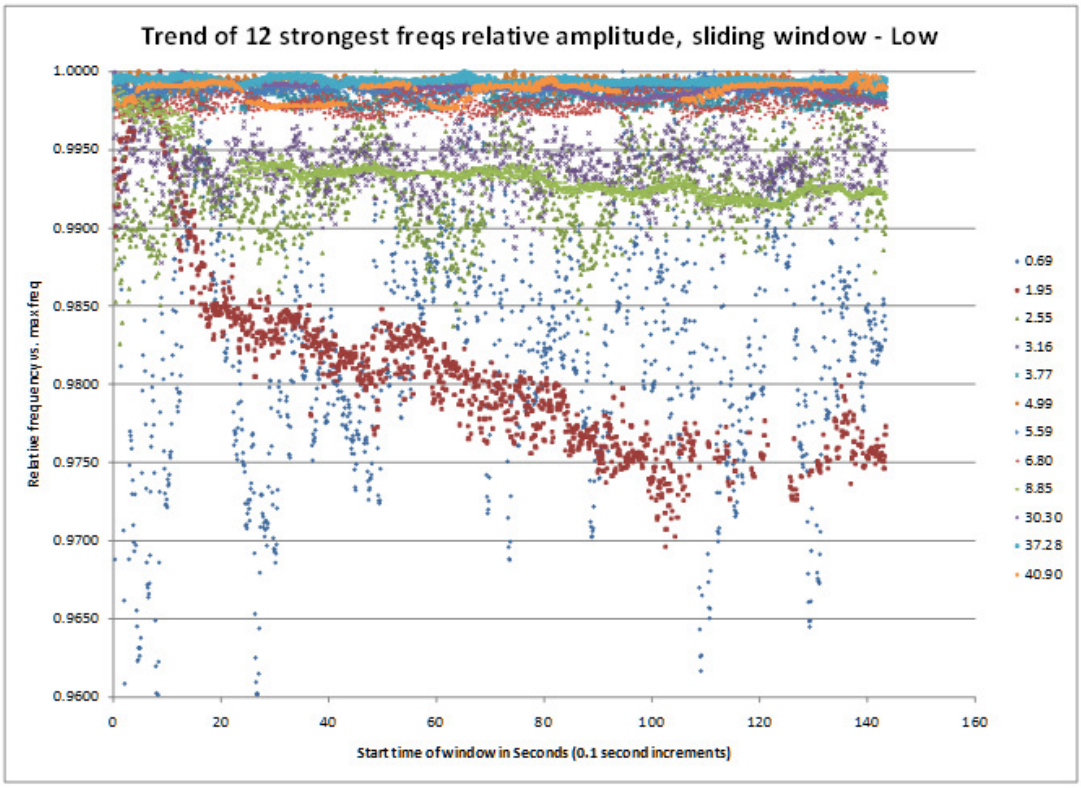

Figure 41: trend of low frequencies over 140 seconds

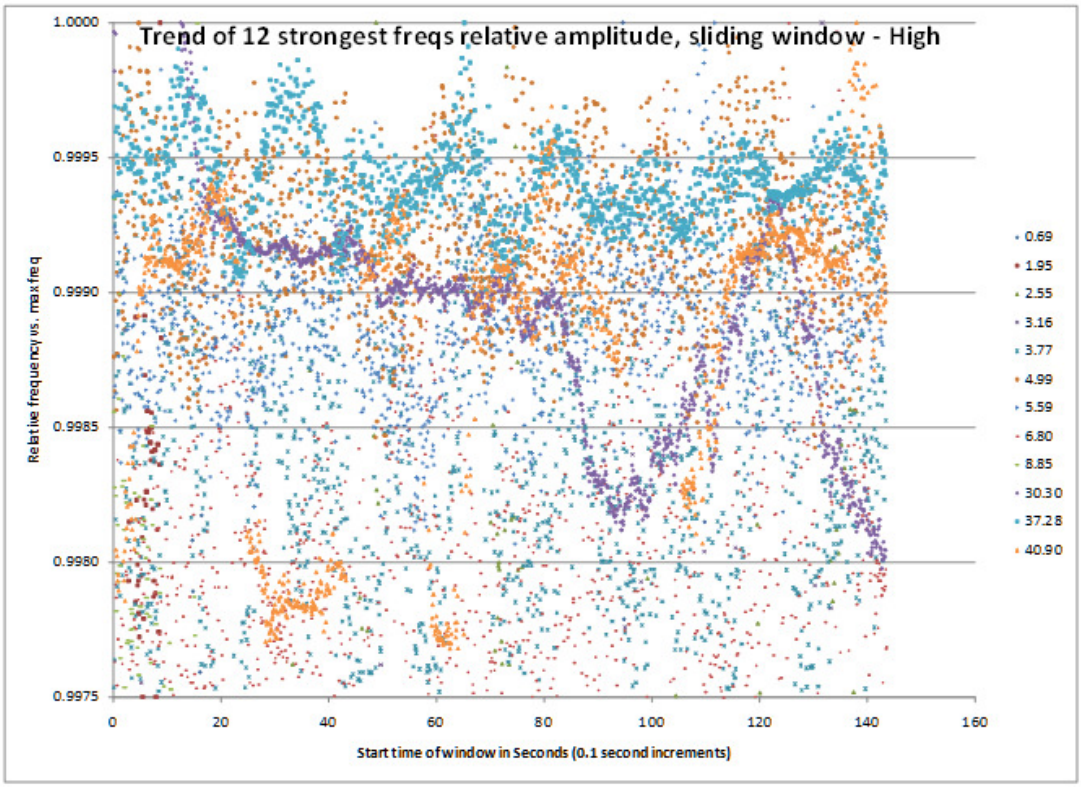

Figure 42: trend of high frequencies over 140 seconds

To examine the relationship of these oscillations to the frequency window values, the standard deviation in relative frequency was taken for 150 iterations and plotted in Figure 43. The standard deviation was highest for the lowest frequencies, falling quickly to a minimum around 5Hz. The standard deviation rose somewhat around 8Hz. This may be related to external driving forces including an 8.42Hz element that was repeated in runs across tension values. The standard deviation towards the top of the spectrum matched the 5Hz low.

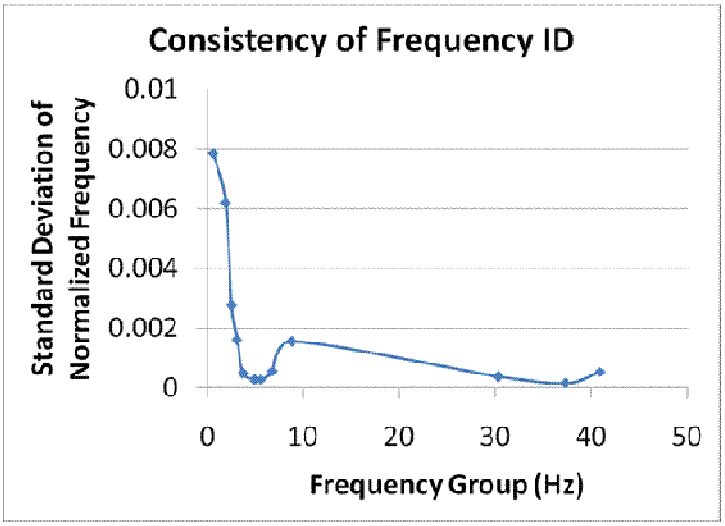

Figure 43: Consistency of frequency identification

The cause of these oscillations was not clear. First suspected were minute vibrations within the Castleman lab, amplified by the small scale of the model cable installation. Passing traffic, wind loads and building fans and other drivers will drive the model and produce fluctuations in its geometry. It is difficult to determine what, if any effects these will have on cable vibrations within the model. Next, aliasing from digital sampling was proposed to explain these oscillations. Aliasing is not clearly related, since its affects should be more pronounced on higher frequencies more than low frequencies. Aliasing effects can be reduced by installing a low pass filter just below the Nyquist frequency on the input signal before the ADC. Our accelerometer has capacitors that filter below 50Hz, while our lab measurement Nyquist frequency was 80Hz, given a 160Hz sampling rate. Finally, limitations in the low frequency performance of the MEMs accelerometer were proposed as an explanation. While the ADXL322 is rated for performance down to 0.5Hz, its sensor is a microscopic mechanical device with minute mass.

Algorithm Performance

The algorithm works well with 8 bits of input variability. With less variability, only higher frequency elements are identified. This is apparent with the original Waterford data, which was gathered using the less sensitive ADXL321 accelerometer with +-18g sensitivity, vs. +-2g sensitivity of the ADXL322. This behavior was also noted using the DSP board on the lab setup, when the input signal was erroneously 1/5 the specified voltage.

9. Castleman Lab Setup

The current lab setup was constructed in the Castleman lab at the University of Connecticut. There were several conditions that needed to be met by this setup for. The base of the structure needed to be movable in order to simulate different horizontal spans between the base of the test cable and its top. The exact unstrained length of the cable needed to be measurable to approximately 1/16th of an inch for Dr. Russell's 'known unstrained length' method. The tension of the cable had to be converted into a force applied directly in series with the force transducer. These conditions were met using the following lab setup.

The top end of the test cable is wound around the end of the c-clamp, which is attached to an I-beam, with the final portion taped. The tape allows for exact knowledge of where the test length of the cable begins off of the c-clamp.

For the base of the cable, an aluminum structure was made. The baseplate of this structure was ½" thick aluminum, over a foot in length, and about 5" in width. The additional area of the base plate was necessary in order to be able to place extra masses on the base plate to weight it down. This allowed the structure to be movable, yet create a rigid test setup when needed by relying on the static friction between the cement floor and the aluminum baseplate. Three additional ½" thick, 1 foot in length, and 2" wide bars were welded together to form the base structure shown in Figure 16. In the center of the base plate, the plate was tapped to allow the force transducer to thread into it rigidly. Directly above the tapped hole, an 1/8" diameter hole was drilled in the top of the base structure. The test cable was bent through the 1/8" hole in the top of the structure. This allowed the tension of the cable to be converted into a vertical force applied through a connecting block (described further below) onto the force transducer screwed into the base plate. It is theorized that the frictional effects of the test cable being bent through the hole in the top of the base structure will be negated by giving the test cable a large excitation around this point (allowing for the test cable to slip around the bend as necessary to create equal tension on both sides of the bend). Current results show that the friction effect of this is negligible due to the lack of precision with the device (only accurate to +/- 1 lbf).

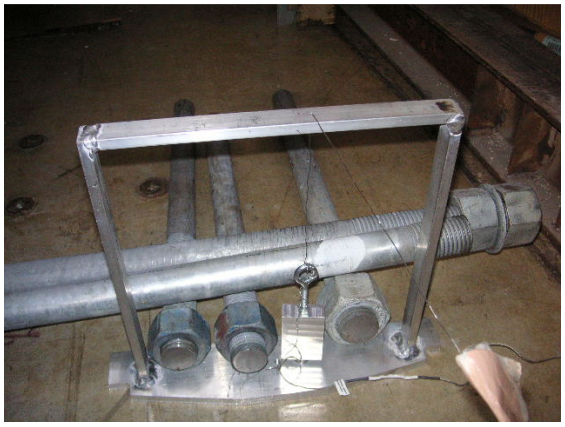

Figure 44: The base structure of the lab setup. The large metal poles were used to weigh the structure down.

The force transducer used is an Omega LC201-50 (Figure 17). It is capable of measuring forces of up to 50 lbf with an accuracy of 1.0% of the full scale output.

Figure 45: Omega LC201-50 Force Transducer

The connecting block is a 6” by 3” by 2” aluminum block that was milled so as to be very flat and very smooth. Both ends of the block were tapped, one end to screw into the other end of the force transducer, and the other end to allow a rigid hook to screw into the block. The bottom end of the test cable, having been bent through the hole in the top of the base structure, is wrapped around this hook.

The test cable is a 45’ long 28 gauge steel cable. This cable, shown in figure … has had masses added to it. This was done to turn the cable into a scaled down model of an actual guy cable. Some of the mechanical properties of the cable are shown in Table 1 below.

Parameter	Symbol	Units	Value
Modulus	E	ksi	16,900
Area	A	in^2	0.001046
Weight Density	D	lb/in^3	11.38

Table 1: Cable mechanical properties

This lab setup has served several purposes. The primary purpose was providing proof that Dr. Russell’s algorithm works. This has been somewhat confirmed not only by using the test cable as a model guy wire, but also through using a guitar string, one of the most tested types of cables for vibration-tension analysis.

A final purpose is to determine how well the algorithm handles temperature change in the test cable. The team intends to compare results from daytime (normal temperature) testing of the cable to results from nighttime (cold temperature) testing of the cable. This drop in temperature will shorten the unstrained length of the cable, and thus will increase the tension. This data has not yet been collected.

Lab Setup Calculations:

There are several calculations that have been done to confirm the veracity of the test setup. These are detailed below.

One of the first tests that needs to be performed is that of determining the static friction coefficient (k) between the concrete floor of the test lab and the aluminum base plate of the base structure. This will be accomplished via the following method:

The force transducer shall be attached to the side of the base structure. The force it takes to drag the base structure will be measured by the force transducer. This will be repeated for varying amounts of weight placed on the base structure, making sure that the weights do not slip. Thus, the coefficient of friction will be calculated via the following formula:

$$k = \frac{f}{W} \qquad (1)$$

where f is the measured frictional force and W is the total weight of the base structure. Calculating this coefficient will allow the team to know how much weight needs to be placed on the base structure to ensure a no slip condition.

The tension at the bottom of the cable (Tb) can be measured via the following equation:

$$T_b = \frac{F}{A} \qquad (2)$$

where F is the cable force measured by the force transducer and A is the unstrained area of the cable.

The tension at the top of the cable (Tt) can be calculated via the following equation:

$$\mathrm{T_t} = T_b + L * A * \rho * g \qquad (3)$$

where L is the unstrained length of the cable and ρ is the density of the cable.

Another factor that must be considered is the deflection of the aluminum support beams in the base structure due to the bending moment of the tension. This must be examined to determine if there will be a significant impact on the horizontal span between the two points of the cable. In this case, only one of the beams needs to be considered as the dimensions and properties for both beams are the same, as would be the bending moment due to the tension of the cable. The first thing to calculate is the bending moment.

$$M = F * \cos(\theta) * 12 inches \qquad (4)$$

Where theta is the angle made between the bottom test end of the cable and the base structure.

The beam is modeled as a cantilevered beam with a moment load, which yields the following equation

$$y = \frac{M * (12inches)^2}{2EI} \quad (5)$$

Plugging in equations 4 and 2 yields the following

$$y = \frac{F}{A} * \cos(\theta) * \frac{(12inches)^3}{2EI} \quad (6)$$

This equation will allow the team to calculate the deflection along the horizontal span due to bending. Using a theoretical maximum force of 50 lbf and a maximum case angle theta of 15 degrees, and a modulus of elasticity of 10^7 psi for the aluminum bars, a theoretical maximum case deflection was calculated to be y = 0.013852 inches. Thus, the bending deflection is considered insignificant.

Lab Setup Results:

Initially, a simple test was performed in order to efficacy of the test setup. A simple metal cable was used instead of the model guy cable. The cable was tightened to different tensions, and the team's accelerometer was used to capture vibration data at each tension. Due to the simplicity of this setup, the following equation was used to theoretically determine the fundamental frequency of the cable at each tension.

$$\omega_i = \frac{i\pi}{L}\sqrt{\frac{T}{\rho}} \tag{7}$$

Where 'i' was equal to one. FFT's were taken from the vibration data, with the results displayed in table 2 below. Uncertainty analysis was also performed on the theoretical natural frequency equation, also displayed in table 2 below. The measured natural frequency results were assumed to be accurate within +/- 1 Hz.

Tension (Pa)	Measured Nat Freq (Hz)	Theoretical Nat Frequency (Hz)	Uncertainty
65069.30953	9	11.77182185	0.08075649
97603.9643	14	14.41747844	0.04454308
108448.8492	15	15.19735666	0.03826341
184363.0437	20	19.81492882	0.01848867
357881.2024	29	27.60736936	0.00922526
607313.5556	35	35.9635098	0.00697206
1051953.837	46	47.33189833	0.00622055

Table 2: This table shows the measured natural frequency and theoretical natural frequency corresponding to a tension the simple cable was tightened to. It also shows the calculated theoretical natural frequency.

A graph of results, including uncertainty analysis error bars is presented below.

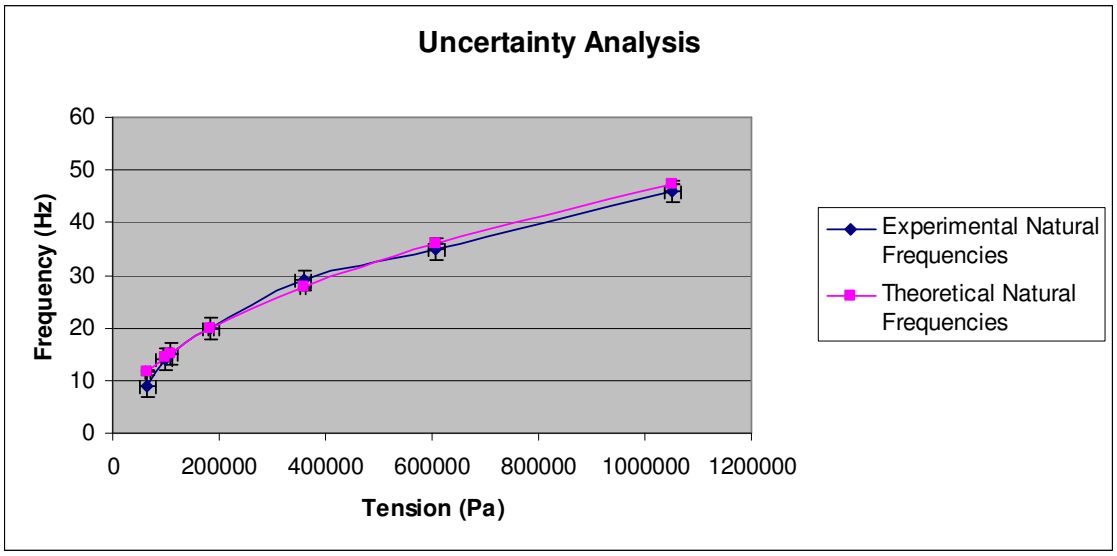

Figure 46: Simple cable test results including uncertainty analysis

These results indicate that the test setup works well for the simple cable test case. However, upon performing actual tests, some limitations to the test setup were discovered. There appear to be environmental factors in the Castleman lab which induce natural frequencies appearing in the results that are not inherent to the cable. A comparison example of the natural frequencies predicted by Dr. Russell's algorithm and those actually discovered is shown in figure 19 below.

Natural Frequency	1st	2nd	3rd	4th	5th	6th	7th	8th
32 lbf Results	2.471	3.670	4.849	6.036	7.255	8.436	9.609	15.474
31.9 lbf Prediction	2.408	3.604	4.757	5.858	6.798	10.058	10.533	11.392
43 lbf Results	1.467	2.894	8.451	11.250	40.936	59.648	78.367	78.920
43.1 lbf Prediction	1.484	2.714	4.059	5.362	6.602	7.661	11.354	

Figure 47: Results from test setup. The yellow box is a frequency that has been consistently found in test data, it is most likely induced by a ceiling fan in the building. The green boxes show a frequency match out of the predicted order. It is most likely to the accelerometer being placed on a node of the model guy cable.

These results show that there is strong correlation between in the predicted results and the actual results, however, it appears that the accelerometer is not picking up some of the predicted frequencies. This may be due to the accelerometer being placed on a node in the cable. However, further testing is required to confirm this. At this point, the team would like to confirm the algorithm on an actual guy cable to prevent any possible environmental factors in the lab from distorting the results.

10. Broadcasting Tower Testing

Using the prototype design that had been assembled, the team visited a broadcasting tower in Waterford to obtain data. Two main problems were identified during this visit.

1. A device would be needed to attach the accelerometer to cables that were out of reach. This is discussed in a previous section of the report.
2. The initial accelerometer obtained by the team measured to large of a spectrum to be useful for the team's purposes. The data obtained by the accelerometer is shown in Figure 20 below.

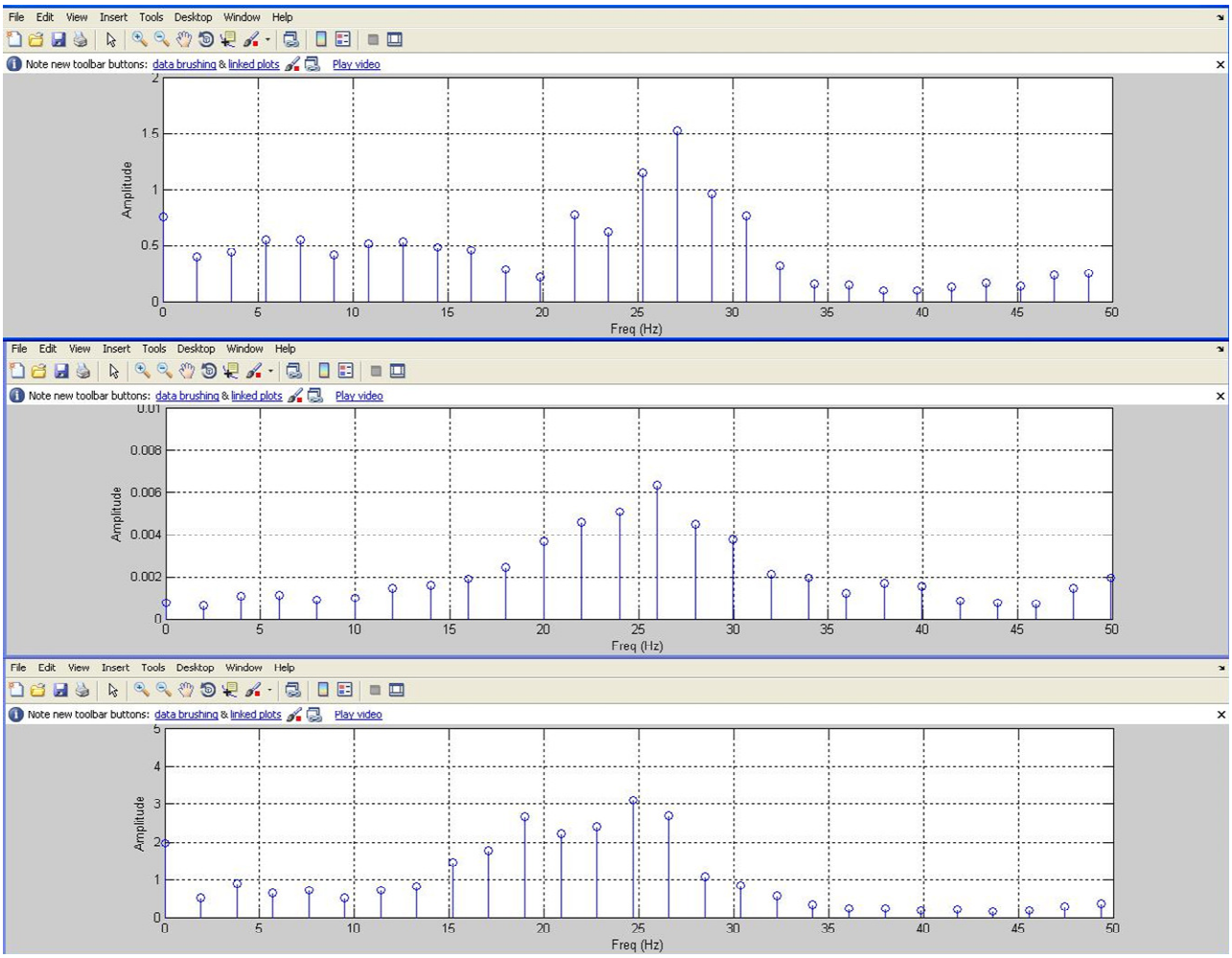

Figure 48: Frequency response data obtained from the Waterford tower. As can be seen by the spacing of the results, the spectrum covered by the accelerometer (0 to 18g) is too large

11. Budget

To-date expenditures of the team:

Item	Amount
Analog Devices ADXL32X Accelerometer	$58.90
BNC breakout cable	$1.95
PicoScope 2203 PC oscilloscope	$245.56
Shipping	$3.22
Total:	**$310.58**

Table 3: To-date expenditures of the team

12. References

1. Russell, Jonathan C. Statics and Dynamics of Tall Guyed Radio Navigation Towers. May 1995.

2. Irvine, Max H. Cable Structures. Cambridge, Mass: MIT Press, 1981.

3. Kitchin, Charles, Mike Shuster, and Bob Briano. "Reducing the Average Power Consumption of Accelerometers." Analog Devices. 08 December 2009 <http://www.analog.com/static/imported-files/application_notes/320665656385 11AN-378.pdf>

4. Budynas, Richard G., and J. K. Nisbett. Shigley's Mechanical Engineering Design. 8th ed. New York, NY: McGraw-Hill, 2008.

5. Russell, Jonathan C., and T. J. Lardner. "Experimental Determination of Frequencies and Tension for Elastic Cables." Journal of Engineering Mechanics. (October 1998): 1067-1072.

6. Starossek, U. "Cable Dynamics - A Review." Structural Engineering International. 171-176.

7. Ren, Wei-Xin, Hao-Liang Liu, and Gang Chen. "Determination of Cable Tensions Based on Frequency Differences." Engineering Computations. 25.2 (October 2007): 172-189. 09 December 2009 <www.emeraldinsight.com/10.1108/02644400810855977>.